Geomorphic expressions of active rifting reflect the role of structural inheritance: A new model for the evolution of the Shanxi Rift, North China

5 Malte Froemchen[1], Ken J. W. McCaffrey[1], Mark B. Allen[1], Jeroen van Hunen[1], Thomas B. Phillips[1], Yueren Xu [2]

[1]Department of Earth Sciences, Durham University, Science Labs, Durham, DH13LE, UK;
[2]Key Laboratory of Earthquake Prediction, Institute of Earthquake Forecasting, China Earthquake Administration, Beijing, China

Correspondence to: Malte Froemchen (malte.froemchen@durham.ac.uk)

Abstract. Many rifts are influenced by pre-existing structures and heterogeneities during their evolution, a process known as structural inheritance. During rift evolution, these heterogeneities may aid rift nucleation, growth, and segmentation of faults, encourage linkage of various segments, or even inhibit the formation of faults. Understanding how structural inheritance

15 influences early rift evolution could be vital for evaluating seismic risk in tectonically active areas. The Shanxi Rift in the North of China is an active rift system believed to have formed along the trend of the Proterozoic Trans North China Orogen. However, the influence of these pre-existing structures on the present-day rift architecture is poorly known. Here we use tectonic geomorphological techniques, e.g., hypsometric integral (HI), channel steepness (ksn) and local relief to identify the impact of structural inheritance on the formation of the Shanxi Rift. We found that HI was less sensitive to lithology and

20 may be more valuable in evaluating the tectonic signal. Based on their geomorphic expression we characterise the activity levels of active faults and found that activity is concentrated in the Rift Interaction Zones (RIZs) that formed in between the sub-basins. Furthermore, we found that many faults formed parallel to inherited structures. Based on these observations we propose a new model for the evolution of the Shanxi Rift where inherited structures play an important part in segmenting the rift. Geomorphic indices might prove useful in the study of the evolution of structural inheritance in other active rifts, such

25 as the East African Rift.

1 Introduction

Many continental rifts exploit ancient orogenic belts to accommodate extensional strain. Examples include East Africa (Rosendahl, 1987; Morley, 1988; Ring, 1994), Baikal (Petit et al., 1996), and the Rhine Graben (Schuhmacher, 2002). Research has focused on understanding the relationship between old inherited structures and the development of younger

30 structures. Pre-existing orogenic belts influence the accommodation of younger episodes of extensional strain, due to the presence of discrete and mechanically weak structures, such as shear zones and associated metamorphic fabrics (McCaffrey, 1997; Phillips et al., 2016; Fazlikhani et al., 2017; Kolawole et al., 2018; Peace et al., 2018a; Heilman et al., 2019), pre-

existing fault networks (Holdsworth et al., 2001b) or lithological contacts (Wedmore et al., 2020a; Phillips and McCaffrey 2019). These mechanical strength contrasts are enhanced when orogenic belts are adjacent to cratons (Dunbar & Sawyer, 1988; Ziegler and Cloethingh, 2004; Corti et al., 2013) as is the case for the Baikal Rift (Petit et al., 1996), the East African Rift (Versfelt and Rosendahl, 1989) and the circum Ordos rifts in North China (Xu and Ma, 1992; Su et al., 2021), because cratonic lithosphere is more resistant to deformation than younger orogenic belts.

Studies of the interaction between rift-related normal faults and inherited structures in offshore basins and margins makes use of the time/space properties of high resolution 2D and 3D seismic reflection data (Morley et al., 2004; Phillips et al., 2016; Peace et al., 2018; Mulaya et al., 2022). Detailed field studies, on the other hand, can resolve the kinematic response of faults and infer strain field directions and interactions (e.g., East Africa, Hodge et al., 2018b; Wedmore et al., 2020; Heilman et al., 2019; Kolawole et al., 2018). Inherited structures and heterogeneities can influence the location, morphology, segmentation and orientation of an entire rift zone (Wilson et al., 1966; Tommasi and Vauchez, 2001; Şengör et al., 2018; Schiffer et al., 2020; Heron et al., 2019). They can also influence the geometry and kinematics of individual faults (Wedmore et al., 2020a; Samsu et al., 2020; Wilson et al., 2010). Inherited structures can influence the development of rifts and their associated basins by controlling linkage of fault segments (Brune et al., 2017; Heilman et al., 2019). Inherited structures have also been shown to act as barriers to rift faults if they form structures or regions of strengthened crust that is harder to deform than surrounding areas (Krabbendam, 2000; Phillips and McCaffrey, 2019).

Many rifts that show a strong signature of ~~inheritance~~ influence are very segmented and exhibit numerous faults and sub-basins that vary in orientation and morphology (Reeve et al., 2015; Morley et al., 2017; Heron et al., 2019; Osagiede et al., 2020). Between individual sub-basins a complex deformation zone known as an accommodation zone or Rift Interaction Zone (RIZ) may develop (Rosendahl, 1987; Morley, 1990; Kolawole et al., 2021). The morphology of these zones is principally controlled by the separation distance between fault segments, the polarity of the respective faults and the amount of overlap between them (Morley, 1990; Faulds and Varga, 1998; Zwaan and Schreurs, 2017; Zwaan et al., 2016). Commonly, these zones are topographically distinct from the rest of the rift. RIZs may form topographic highs in their early evolution, ~~that~~ form a drainage divide between depocenters (Ebinger et al., 1987; Lambiase and Bosworth, 1995; Gawthrope and Hurst, 1993), and therefore act as a source ~~for~~ sediment (Gawthrope and Hurst, 1993; Scholz 1995). As these zones evolve, they can become breached and eventually link up the rift basins (Kolawole et al., 2021). These zones may show a perturbated local strain field due to the influence of the adjacent bounding rift faults (Crider and Pollard, 1998; Kattenhorn et al., 2000; Maerten et al., 2000) and ~~an~~ underlying inherited structures which may cause the strain field to rotate (Morley, 2010). Development of these zones may be aided by oblique striking basement fabrics (Fossen and Rotevatn, 2016); however, basement fabrics may also influence linkage across these zones (Morley et al., 2004; Heilmann et al., 2019). RIZs are important zones of rift systems and inheritance may be key to understanding their geometry and evolution.
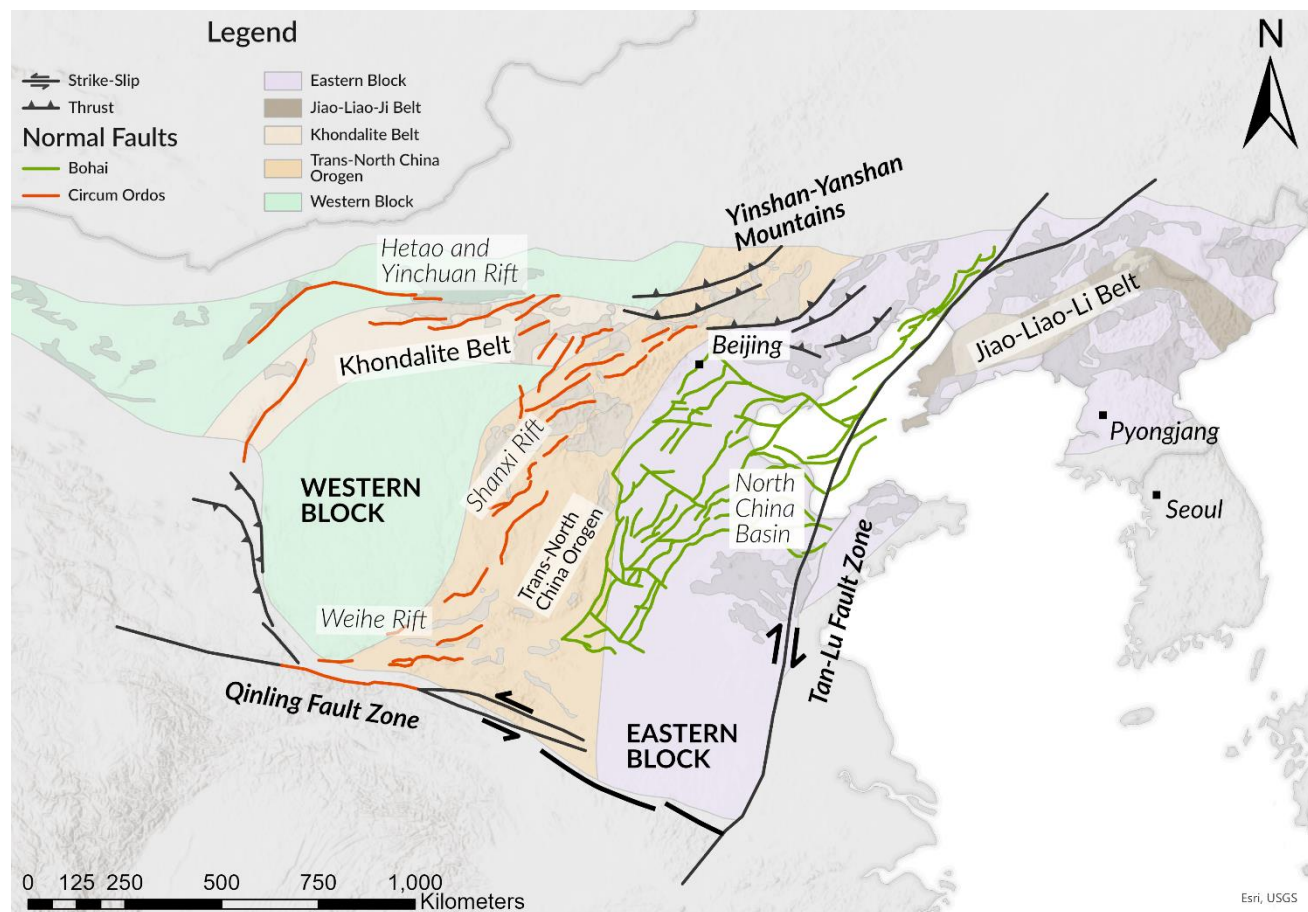
Figure 1: Overview map of the North China Craton (NCC) with boundaries of the different blocks and orogenic belts that make up the NCC shaded in colour. Boundaries after Zhao et al. (2005). Also indicated are the two major rift systems that formed superimposed on the NCC: The Paleogene North China Basin (in green, modified from Qi and Yang, 2010) and the largely Neogene Circum Ordos Rifts (in red, modified from Zhang et al. 2003, Deng et al. 2007). Bold black lines indicate the major strike slip fault zones that effect present-day deformation.

The Shanxi Rift in North China contains faults with a variety of trends which formed in the Late Miocene to present day (Su et al. 2023) (Fig.1). The origin of these trends is unclear to this day. They may have formed through frequent stress changes during the evolution of the Shanxi Graben, with the strain ~~during transtension~~ being partitioned as both dip-slip and strike-slip faults (Shi et al., 2015a). There has been little focus on the influence of structural inheritance in the wider evolution of North China, with a few exceptions (Pavlides et al., 1999; Su et al., 2021). Major faults in the Shanxi Rift commonly expose basement massifs of the Trans North China Orogen (TNCO) in their footwalls. The TNCO formed during the collision of the Eastern and Western Block of the NCC in the Paleoproterozoic. While these basement massifs have been intensively studied to unravel the exact timing and kinematics of the Proterozoic collision (Zhao et al., 2001a; Kusky and Li, 2003; Trap et al.,

2007; Trap et al., 2008; Faure et al., 2007; Trap et al. 2009a; Trap et al., 2009b; Zhai et al. 2010; Zhai and Santosh, 2011),

80 the role of these basement massifs on the late Cenozoic rifting in the Shanxi Rift has been underappreciated by researchers.

There is very limited seismic reflection data available for the Shanxi Rift (Xu and Ma, 1993; Ai et al. 2019). However, the degree of tectonic activity and subaerial exposure makes it possible to use geomorphology to study the structural evolution. In subaerial, exposed active rifts geomorphology and surface expression of faults is a commonly used tool that has been successfully employed in regions such as the Basin and Range (Jackson and Leeder, 1994; Densmore et al., 2003; Densmore

85 et al., 2004), the Apennines (Whittaker et al., 2008; Geurts et al., 2020) the Gulf of Corinth (Leeder and Jackson, 1993; Goldsworthy and Jackson, 2000) or the East African Rift (Erbello et al., 2022; Dulanya et al., 2022). These geomorphic approaches are varied and include studying the drainage evolution, the topographic response to faulting or using rivers to track the transient uplift rate. Landscapes are primarily formed by two competing forces: tectonics and erosion (Whittaker et al., 2012). Geomorphic indices have been created to quantify landscape response to tectonics (Bull and McFadden, 1977;

90 Cox et al., 1994; El Hamdouni et al., 2008; Gao et al., 2016; Markrai et al., 2022). This study uses three indices to evaluate the landscape response to faulting in the Shanxi Rift: Hypsometric integral, channel steepness and local relief.

By combining geomorphic analysis with analysis of the Pre-Cenozoic structures and geology, we provide new insights on the influence of inheritance on the evolution of the Shanxi Rift. Specifically, we investigate the relationship between the basement heterogeneities and inherited fabrics and the active normal faults to address how the Shanxi Rift was segmented

95 and how inherited fabrics facilitated rifting. Our results question the need for rapid changes in the Neogene strain field to explain the varying fault orientations and fault evolution in the Shanxi Rift. Instead, we show a novel, simpler model that invokes influences of inheritance under a constant strain field. More generally, our work shows how geomorphic indicators can be used to identify the most active (and potentially hazardous) faults in an active extensional system.
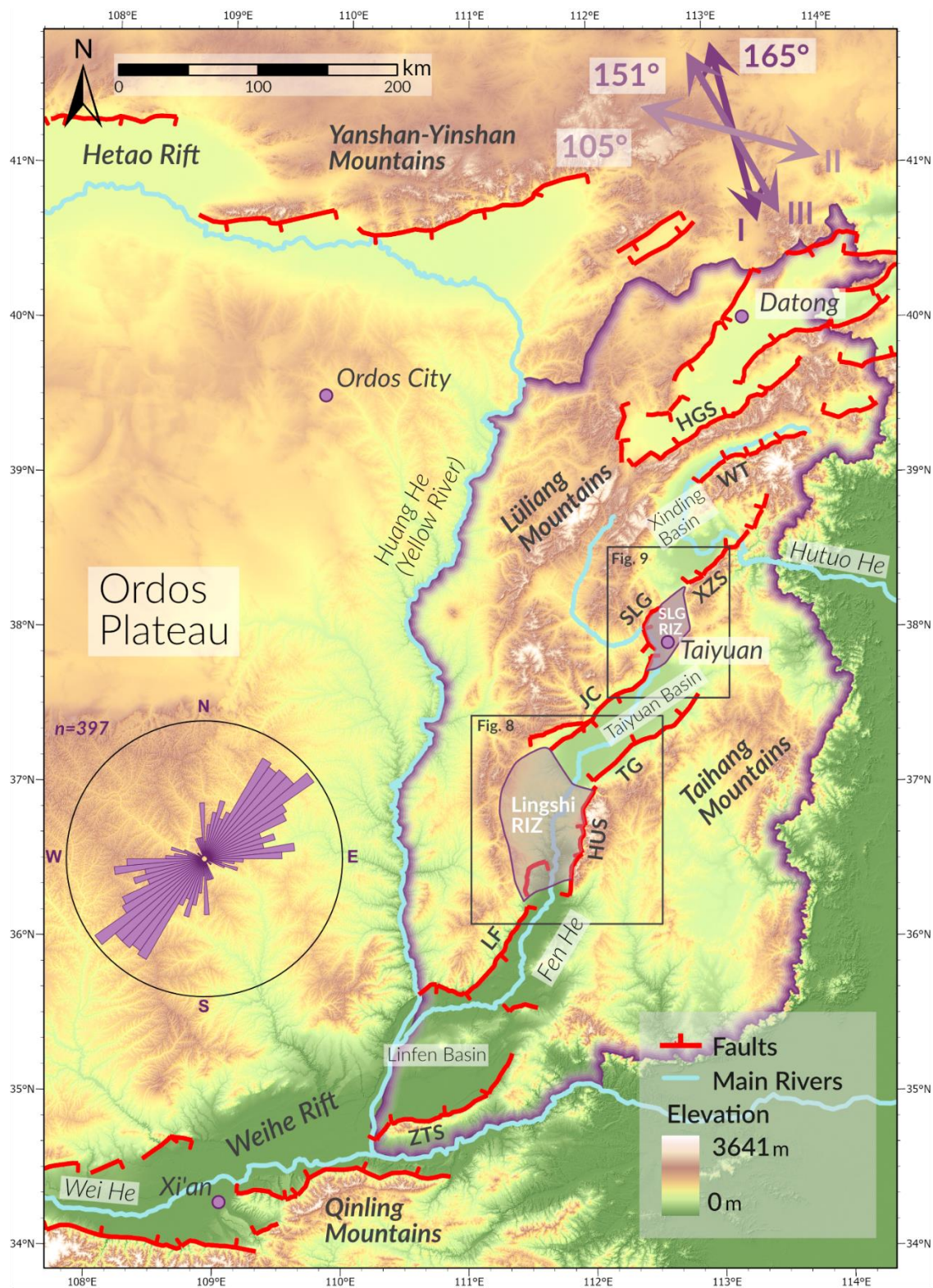
100

Figure 2: Detailed map of the circum-Ordos Rifts and the main rivers (based on Shuttle Radar Topography Mission (SRTM)-digital elevation model (DEM)). Extension directions shown are from: I-- Zhang et al. (1998) II-- Shen et al. (2000) III--Middleton et al. (2017). Rose plot shows the mean orientation of major rift faults in the Shanxi Rift (defined here as the regions that lie within the purple bounding line). Faults were split into individual segments according to their orientation. (Abbreviations:

105 **HGS-Hengshan; WT-Wutai; XZS-Xizhoushan; SLG-Shilingguan; JC-Jiaocheng; TG-Taigu; HUS-Huoshan; LF-Linfen; ZTS-Zhongtiaoshan)**

2 Geological Setting

The Shanxi Rift system in North China is an active continental rift system that is superimposed on the Trans North China Orogen, a Paleoproterozoic Orogen that formed about 1.8 Ga (Fig. 1). The Trans North China Orogen formed during the

110 collision of the Eastern and Western Blocks that formed the North China Craton (NCC). Exact timing and kinematics of this collision remain uncertain (Zhao et al., 2005; Kusky et al., 2007; Zhang et al., 2001; Zhai and Santosh, 2011). Since the Proterozoic, the North China Craton has been a relatively stable cratonic block with a lithospheric thickness of 200 km, evidenced by Palaeozoic kimberlites (Menzies et al., 1993; Griffin et al., 1995). The Paleoproterozoic and Archean basement rocks are covered by low-grade metamorphosed sediments, locally known as the Hutuo Group. Lower Palaeozoic cover

115 consists of Cambrian continental siliclastic successions, followed by shallow marine carbonates and Ordovician platform carbonates. Carboniferous and Permian rocks represent changing shallow marine to fluvio-deltaic conditions and contain coal measures. These are topped by Mesozoic continental clastics, grading into cross-bedded aeolian sequences in the Jurassic (SBGMR, 1989).
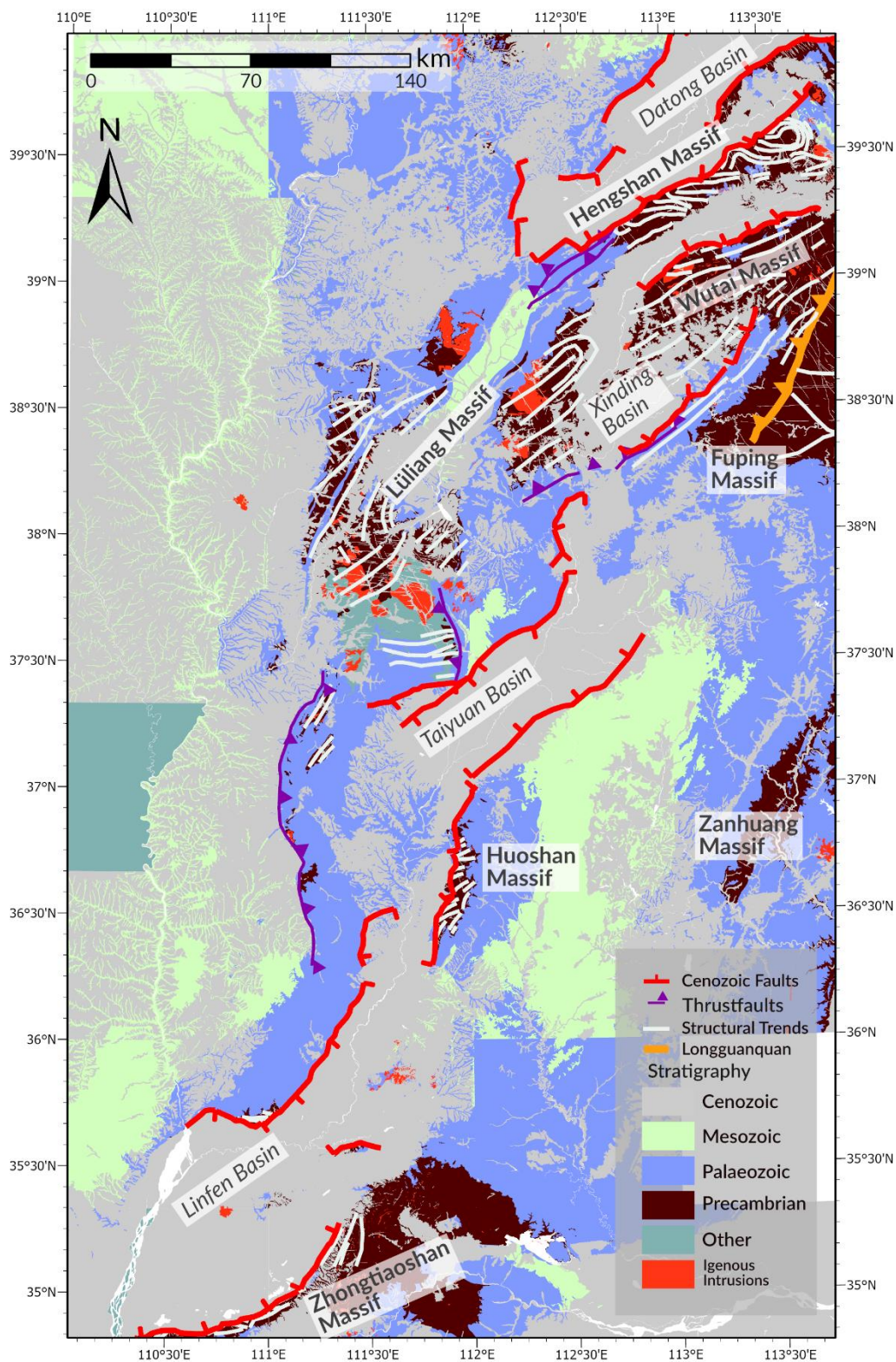
Figure 3: Simplified geological map (modified from SBGMR (1989)) of the Shanxi Rift showing the main structures (Trap et al., 2007; Trap et al., 2009; Clinkscales and Kapp, 2020; Faure et al., 2007; Zhang et al., 2020). Main metamorphic fabrics are indicated in grey lines which are predominantly orientated NE-SW.

Since the Mesozoic, parts of the NCC have been destroyed by thermal erosion (Griffin et al., 1998; Menzies and Xu, 1998)

125 and/or partial delamination (Gao et al., 1998; Gao et al., 2002; Gao et al., 2004) which is likely to be connected to the subduction of the palaeo-Pacific underneath East Asia (Menzies et al., 2007; Zhu et al., 2011). The Eastern and Western part of the NCC underwent a different evolution during the Mesozoic. The Eastern part experienced compressive deformation during the Jurassic to Early Cretaceous (Davis et al., 2001) also regionally known as the Yanshanian Movement (Wong, 1927; Dong et al., 2015) which was less pronounced within the Western Block. However, Paleoproterozoic orogenic belts

130 like the TNCO also record this widespread compressional event (Clinkscales et al., 2019; Zhang et al., 2008). Since the Early Cretaceous the eastern NCC experienced extension, resulting in structures such as pull-apart basins, core complexes and associated voluminous magmatism (Zhu et al., 2012). Mesozoic magmatism almost exclusively affected the Eastern NCC. Destruction of the cratonic lithosphere was limited to the Eastern NCC. Here, the North China Basin formed in the Eocene-Oligocene (Allen et al., 1997). This basin has transtensional kinematics, that gives it a resemblance to a giant pull-

135 apart (Chen and Nabelek, 1988; Farangitakis et al., 2020). The Paleogene was broadly a period of tectonic quiescence in the Western NCC. Since the Neogene localised, narrow rifts which appear to follow the trend of Precambrian orogenic belts within the North China Craton surround the Ordos block (Shi et al., 2020). One of these rift zones is the Shanxi Rift.

The Shanxi Rift is a NE-SW trending rift system that consists of a series of right-stepping en-echelon basins. (Zhang et al., 2003) (Fig. 2a). The system is ~1000 km long and ~300 km wide and is bounded to the North by the Yinshan-Yanshan range

140 and to the South by the Qinling range. It is commonly believed to have initiated in the Late Miocene based on the oldest sediments found in the rift grabens–- the Kouzhai Formation (Xu et al., 1993). The crust beneath the Shanxi Rift is ~32-39 km thick and is thinner in the basinal regions than underneath the Lüliang and Taihangshan highlands, which flank the rift to the west and east (Chen, 1987; Tang et al., 2010). The Shanxi Rift is characterized by a series of distinct rift basins that have either half graben or graben geometries, separated topographically higher elevated areas which have previously been called

145 push-up swells: The Lingshi and Shilingguan (Fig. 3) (Xu and Ma, 1992; Xu et al., 1993). The Linfen Basin to the south is separated by Lingshi RIZ from the Taiyuan Basin which is in turn separated from the Xinding Basin in the North by the Shilingguan RIZ. There are two main rivers that run through the Shanxi Graben: The Hutuo River draining towards the East across the Xizhoushan Fault into the North China plain while the Fen River is diverted to the South where it drains into the Yellow River (Fig. 2) with the main drainage divide between these represented by the Shilingguan RIZ. The Xinding and

150 Linfen basins contain up to 3000-4000 m thickness of sedimentary fill, while the Taiyuan Basin contains ~6000 m of sedimentary rocks (Chen et al., 1987; Su et al., 2023). The rift has produced infrequent but devastating earthquakes in historical time. The AD 1303 Hongdong Earthquake is believed to have been an MW ~7.5 event (Xu et al., 2018) and is well-documented in Chinese historical writings. Shanxi Province itself is densely populated with 36.5 million inhabitants.

Large cities like Taiyuan (5 million inhabitants), Linfen (4 million inhabitants) and Datong (3 million inhabitants) are close to active faults.

Constraining the exact extension direction and rate is difficult due to the low strain rate of the Shanxi Rift. A variety of researchers have used field-based fault slip measurements, GPS derived velocities and/or earthquake focal mechanisms. Studies by Shen et al. (2010), He et al. (2003) and Middleton et al. (2017) constrain the extension direction in Shanxi to an azimuth between 105 and 180° and the extension rate between 0 and 6mm/yr (Fig. 2). Other studies using field-based measurements (Shi et al., 2015a; Assie et al., 2022) propose a complex evolving strain field that has changed throughout the Cenozoic. According to these studies, NW-SE extension in the Mio-Pliocene initiated the rifting in Shanxi and was followed by NE-SW extension in the early Quaternry leading to further subsidence. The current NNW-SSE extension strain field developed at 0.11 Ma which marks a shift to right lateral deformation in the Shanxi Rift, dated using basalts cut by faults (Shi et al., 2015a). Shi et al. (2015b) and Shi et al. (2015a) relate these short-term changes in the strain field to growth of the Tibetan Plateau.

3 Methods

3.1 Pre-Rift Architecture and Structural Analysis

We compiled a map of the ancient and active structures in the Shanxi Rift (Fig. 3) to investigate the influence of inheritance on the active structures in the Shanxi Rift. Ancient structures such as basement fabrics, thrust faults and shear zones were digitalised from published maps in ArcGIS Pro™. Additionally, we compiled the published structural data of the Paleoproterozoic basement complexes and plotted the data on stereonets. To map the active fault structures, we identified linear breaks in the landscape on SRTM topographic data with a 90 m resolution (https://lpdaac.usgs.gov/products/srtmgl3v003/), or on the topography-derived attributes slope and curvature. This resolution is appropriate for the larger regional scale of this study and helps keep computing power demands manageable.

3.2 Geomorphic Indices

We used geomorphic indices to quantify the landscape response of the Shanxi Rift to tectonic drivers. We analysed the morphometric indices from 10873 1st Order drainage basins located in the Shanxi Rift, using the SRTM data. Figure 2 shows a topographic map and location map of the study area. We focused in this study on three geomorphic indices; 1) Local relief, 2) the Hypsometric Integral (HI) and, 3) the normalised channel steepness (k_{sn}), as these proved to be the most helpful and robust when evaluating the tectonic signals.

3.2.1 Local Relief (R_l)

Local relief is commonly used measurement of the variation of topography over an area to analyse spatiotermal tectonic trends (Ahnert, 1970; Schmidt and Montgomery, 1995; DiBiase et al., 2010). The relief R_l was calculated as the maximum

185 difference in elevation E over; 1) a delineated drainage basin (of 1st order – see below) or, 2) within a circular moving window with a 1 km radius:

$$R_l = E_{max} - E_{min} ,$$ (1)

where R_l is the local relief and E refers to elevation. High relief landscapes therefore show a higher variation of elevation over an area which may indicative faster uplift rates.

190 ### 3.2.2 Hypsometric Integral (HI)

The Hypsometric Integral (HI) was first used as a geomorphic index by Strahler (1952). It is a measurement of the distribution of elevation within an area. HI is derived as the integral of the hypsometric curve, which plots normalised elevation over normalised drainage area for each drainage basin. Figure 3 illustrates the theory behind HI. The interpretation of the hypsometric curve assumes that topographically more youthful basins will have a convex-up shaped curve, while more

195 mature ones will have a more concave-up shape. If uplift outpaces erosion there will be a greater range of elevation over an area which results in a convex-up shaped curved and a high HI. Therefore, high HI values should coincide with rapidly uplifting areas (e.g., footwalls of active normal faults) (Chen et al., 2003; El Hamdouni et al., 2008; Perez-Pena et al., 2009a; Obaid and Allen, 2019; Groves et al., 2020; Erbello et al., 2022).
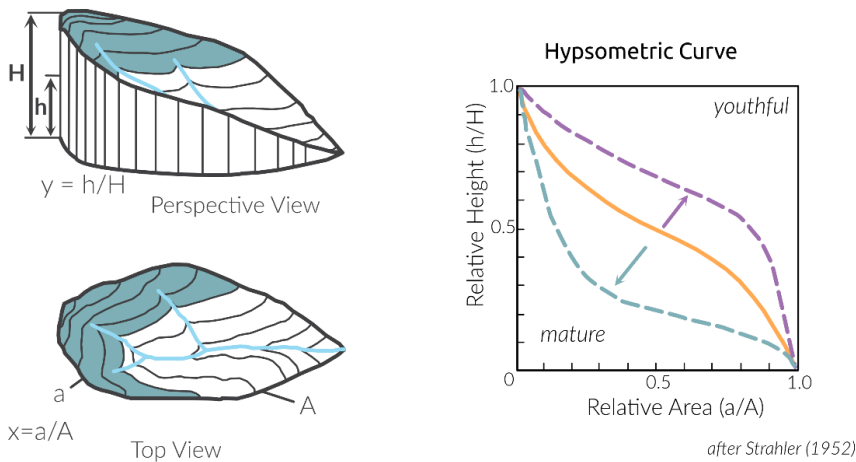
200 **Figure 4: Schematic diagram explaining the concept of the Hypsometric Integral (after Strahler, 1952). Every drainage basin is dissected into elevation bands to determine a ratio of relative height over relative area. Concave curves indicate more youthful topography while convex shaped ones indicate more mature topography.**

In this study we calculated the HI ~~per~~ drainage basin (Obaid and Allen, 2019; Groves et al., 2020). The shape and size of
205 drainage basins is controlled by tectonic and geological features, ~~they are more~~ natural boundaries for comparing areas of
variable uplift and erosion rates than calculating HI with an arbitrary moving window. We calculated the hypsometric curves
using QGIS 3.16 and derived the integral for each curve through an R script (Supplementary material X1). The hypsometric
integral was calculated for 1st, 2nd and 3rd Strahler order drainage basins (Strahler, 1952, 1957).

3.2.3 Normalised Channel Steepness (k_{sn})

210 Normalised Channel steepness (k_{sn}) is a frequently used topographic metric in tectonic geomorphology (DiBiase et al., 2010;
Whittaker and Walker, 2015). For steady-state landscapes, meaning ~~when~~ rock uplift rates and river incision rates are at
equilibrium, the channel slope S is defined as a power law function (Hack, 1957; Flint, 1974):

$$S = k_s A^{-\theta} \tag{2}$$

where A is the drainage area. The parameter k_s is the channel steepness index, and θ denotes the channel concavity index.
215 (Snyder et al., 2000). In natural landscapes, it was found that ~~there exist~~ variations in the best-fit for concavity index ~~(θ)~~
~~which~~ has a significant impact on estimates of k_s, ~~to~~ circumnavigate the problem, we used a reference concavity index of
0.45 (Wobus et al., 2006). Using this reference concavity index ~~makes the resulting value "normalised", now written as k_{sn}~~
~~thus making k_{sn} dimensionless.~~ Variations in k_{sn} along channel segments may be related to changes of the uplift rate of that
region (Whipple and Tucker, 1999; Snyder et al., 2000).
220 We used the TopoToolbox Matlab (Schwanghart and Scherler, 2014) scripts to extract the river profiles and calculate the
normalised channel steepness from smoothed river profiles. This approach is built upon the method developed by Perron and
Royden (2013) to analyse river profiles. We extracted streams with a drainage area of above 1 km^2 to avoid hillslope areas.
Normalised channel steepness (k_{sn}) is commonly applied to stream networks to visualise knickpoints (variations in the slope
of river channels) in rivers. In this study, we used Topotoolbox to calculate a mean value for k_{sn} per drainage basin by taking
225 a mean of the k_{sn} values of all streams in that drainage basins. This makes it easier to compare the k_{sn} values to ~~those for~~ local
relief and HI. The k_{sn} stream network map is available in the supplementary material (S1).

4 Results

4.1 Pre-rift structural architecture

The northern part of the Shanxi Rift is dominated by uplifted Proterozoic basement massifs. The Hengshan, Lüliangshan,
230 Wutai and Fuping massifs are exposed in the footwalls of major basin bounding faults (Fig. 3). In the South, the footwalls are
more commonly dominated by Mesozoic and Palaeozoic sediments, with notable exceptions being the Huoshan and
Zhongtiaoshan faults, which also expose Paleoproterozoic basement at surface.

The general trend of most Paleoproterozoic structures is broadly NE-SW, which is sub-parallel to the active structures. Locally the basement trends have a more ENE-WSW orientation or in the case of Hengshan an E-W trend where a local shear zone dominates the pre-existing fabrics. The orientations also become circular, or dome-like in the basement massifs of the Hengshan and the Lüliangshan mountains. The Fuping massif displays a considerable spread of basement fabric trends that can be split into two groups: fabrics trending NE-SW in the NW and fabrics broadly with an NNW-SSE trend in the SE. These two regions are separated by the NE-SW trending Longguangquan Shear Zone (marked as a purple thrust fault on Fig. 3) which most likely originated as a shallow-dipping thrust fault in the Paleoproterozoic (Trap et al., 2008). The basement fabrics in the NW-part and the Longguangquan Shear zone are nearly parallel to the Xizhoushan Fault. Further North the Paleoproterozoic basement fabrics of the Wutai complex are orientated ENE-WSW which is mirrored by the active normal Wutai fault.
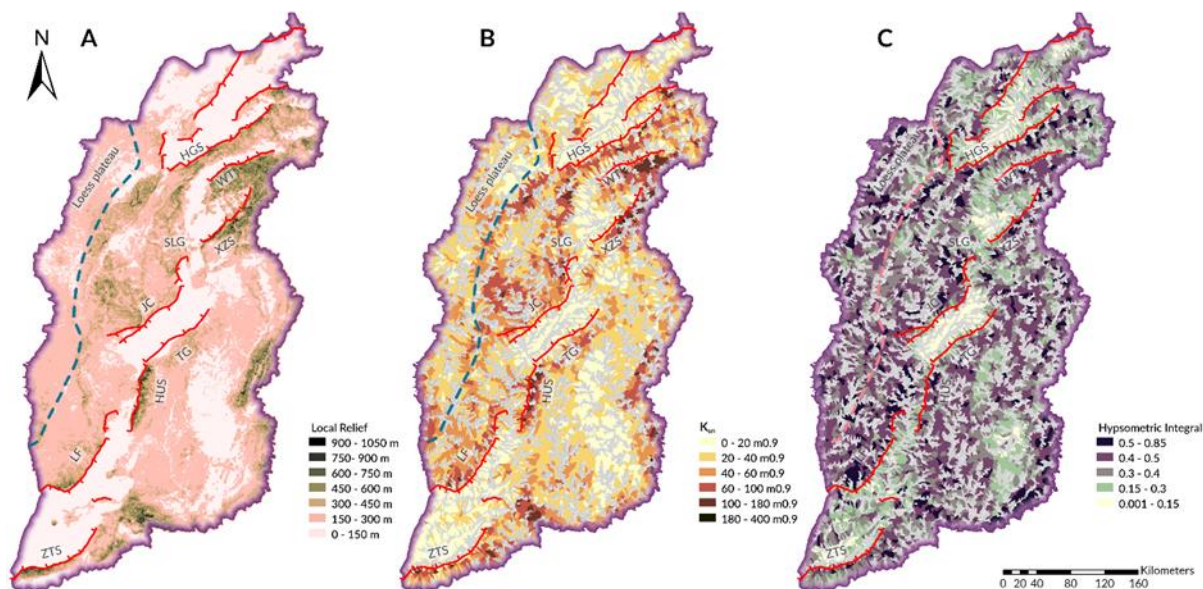
Figure 5: Geomorphic indices map of the Shanxi Rift. Major extensional faults shown in red, boundary of the Loess plateau indicated by dashed line. A) Local relief map. Darker colours indicate higher relief regions. Local relief was calculated within a 1km circular radius. High relief is found especially in the northern Shanxi Rift in the footwalls of the Wutai and Xizhoushan faults as well as further south along the Huoshan and Zhongtiaoshan faults. Noticeably lower local relief values occur along the central Jiaocheng and Taigu faults. B) Mean normalised channel steepness (ksn) calculated for 1st Strahler order basins. High values are commonly located in the footwalls of active faults, especially the Wutai, Xizhoushan and Huoshan faults. Low values are found in the lower lying basin regions. Central faults (Taigu and Jiaocheng) show noticeably less high k_{sn} basins than other faults. C) Hypsometric Integral (HI) calculated for 1st Strahler order basins. High values are commonly located in the footwalls of active faults, especially the Wutai, Linfen, Shilingguan and Huoshan faults. Low values are found in the lower lying basin regions. Central faults (Taigu and Jiaocheng) show noticeably less high HI basins than other faults.

(Abbreviations: HGS-Hengshan; WT-Wutai; XZS-Xizhoushan; SLG-Shilingguan; JC-Jiaocheng; TG-Taigu; HUS-Huoshan; LF-Linfen; ZTS-Zhongtiaoshan)

4.2 Relief

The local relief of the region (Fig. 5a) closely follows the overall topography of the region but emphasises certain features to make them easier to identify. Two areas of high local relief can be identified in the North and South of the Shanxi Rift.

In the Northern region around the Wutai and the Xizhoushan faults the footwalls of the prominent bounding faults are highly

260 elevated (2500-3000 m) and show local relief values exceeding 1000 m. In the southern part of the Shanxi Rift, the Huoshan Fault to the South also shows high local relief (>1000 m) in the footwall close to the bounding fault. The Zhongtiaoshan Fault is a more complicated case as the local relief is high (>1000 m) along the western end of the fault but falls to 300-400 m towards the east. The other high relief faults in Shanxi show a more consistent high local relief pattern along their fault traces.

265 The Shilingguan RIZ is characterised by shorter faults segments and this region shows an elevated local relief of around 500 m. In some examples, in footwalls close to the main fault the local relief exceeds 1000 m. This is seen where a broadly N-S trending fault and a broadly NE-SW trending fault intersect and possibly link up. Further into the footwall of this fault there are pockets of high (>1000 m) local relief, which are along the sides of the narrow gorge of the Fen River. Compared to faults in the North and South of the Shanxi Rift such as Huoshan, Zhongtiaoshan or Wutaishan, the elevation in this area is

270 lower (~1500 m) but the local relief remains comparatively high (up to 1000 m). The two longest faults in the central region of the Shanxi Rift, that bound the Taiyuan Basin (Taigu and Jiaocheng) only show a lower local relief response rarely exceeding 450 m, with elevation lying between 1500 and 2000 m.

There are regions of medium-high values of local relief (450-750 m) away from active structures for example in the Taihangshan mountains or to the West of the Lingshi RIZ. These match up with older contractional structures and are

275 interpreted to be remnants of earlier tectonic events that created high standing topography.

4.3 Normalised channel steepness (k_{sn})

Four regions show high basin averaged k_{sn} values (Fig. 5b): The Huoshan Fault, the Xizhoushan Fault (especially its more eastern part), the Wutai Fault and the Zhongtiaoshan Fault. These are the same regions that also show high relief. Low values of less than 50 are rarely associated with obvious faults with a surface trace. However, the main bounding faults of

280 the Taiyuan Basin, the Jiaocheng and the Taigu faults, show a wide range of values with most basins lying in the 50-85 region, which matches with their generally lower values on local relief maps. The footwall of the fault bounding the Shilingguan RIZ shows elevated values. Especially the area where the broadly NS and NE-SW trending faults link up show basins with k_{sn} exceeding 100.

4.4 HI

285 While the Local Relief and the Channel Steepness showed broadly similar distributions, the Hypsometric Integral differs slightly and shows a more distributed pattern of high (>0.5) HI basins (Fig. 5c). The footwall blocks to the Wutai,

Xizhoushan and Zhongtiaoshan faults show elevated responses but in contrast to the previously described geomorphic parameters they do not show the highest values. In the footwalls of these faults, HI values mostly range between 0.3-0.5 and only isolated regions go above 0.5. The highest values are found along the Huoshan Fault and along the footwall of the
290 bounding fault of the Shilingguan RIZ. Here values commonly exceed 0.5 and rarely are below 0.4. These high HI values match spatially with the high channel steepness and k_{sn} values. Therefore, they have consistently higher values compared to the Wutai, Zhongtiaoshan or Xizhoushan footwalls. The Lingshi RIZ that is bounded by the Huoshan Fault also shows elevated values compared to the surrounding basins, due to its overall higher elevation and dissected topography. The Taigu and Jiaocheng faults have generally lower HI values (below 0.4), matching the low values for channel steepness and local
295 relief.

High value HI basins (>0.5) are also found in regions away from the active normal faults that showed no recent tectonic activity. High values are observed to the west of the Shanxi Rift in the Loess Plateau on the western edge of the HI map. (Fig. 5c) This is due to the landscape that typifies the Loess Plateau west of the Shanxi Rift. Due to the Loess being relatively unconsolidated sediment it is prone to dramatic erosion that creates deep gullies and ridges which can lead to high
300 HI values. The Loess Plateau formed in the Pleistocene and its linear ridges and gullies have been carved out by aeolian and fluvial forces (Kapp et al., 2015) since therefore in a way it signifies youthful landscapes just not one shaped by tectonic forces. Similar to the relief and the channel steepness, high values are also observed in high elevation regions further away from mapped active faults. These commonly correspond to known thrust faults or other contractional structures (SBRGM, 1989) which were last active in the Mesozoic and created relict topography. This shows the limitations of HI as sometimes
305 regions of HI values may not correspond to active tectonic structures but are related to palaeotopography or loess landscapes.

4.5 Distribution of geomorphic values across faults

Using R we also generated violin plots that visualise the distribution of values for each geomorphic index. The shape of the "violins" represents the distribution of values as the violin will be thicker the more data points sit at that range.
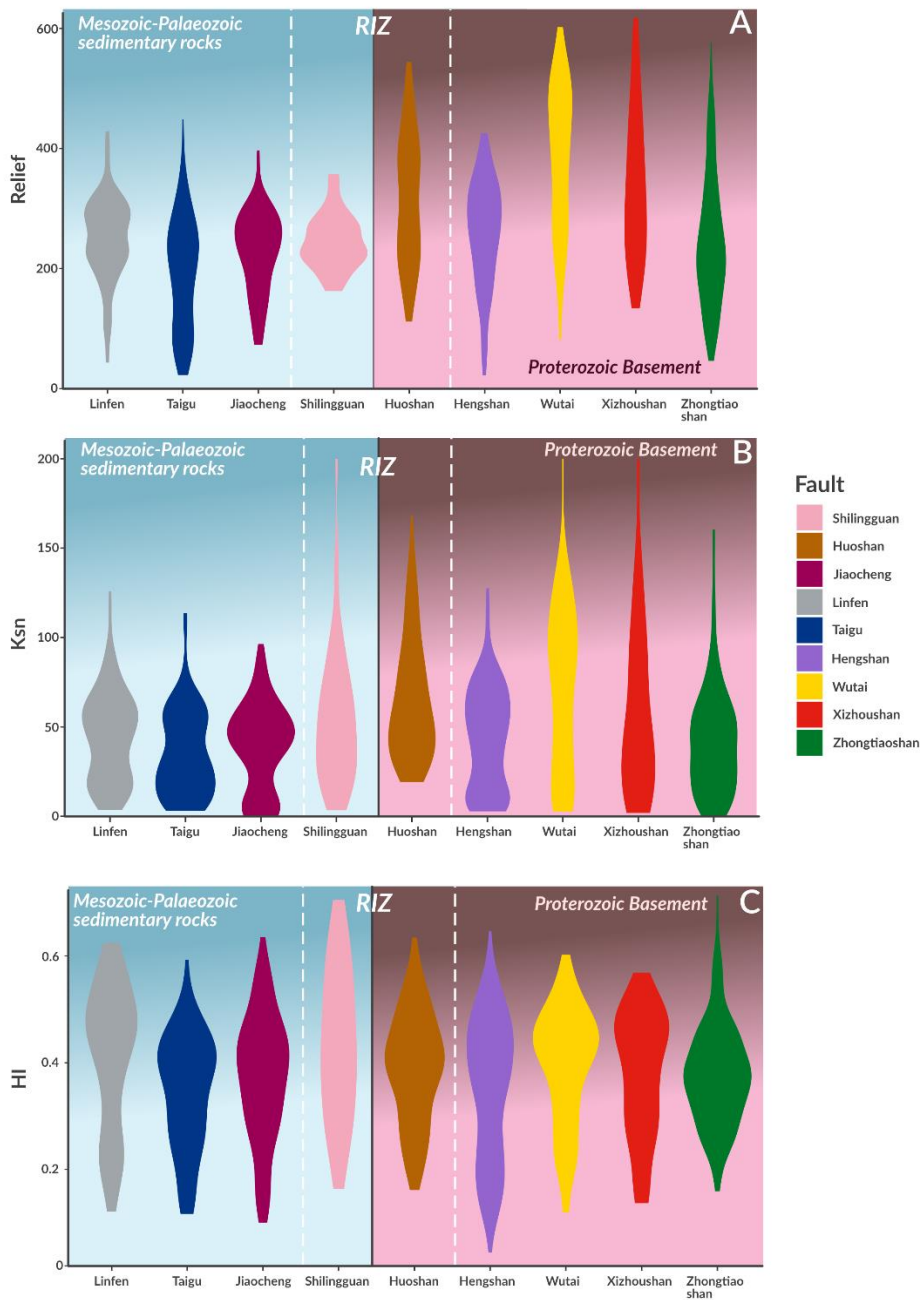
310

Figure 6: Violin plots showing the distribution of geomorphic values for each fault. Background shows the dominant footwall composition of the faults with RIZ faults being highlighted in the middle. A) Relief. Clear separation of faults with high values all having Proterozoic basement-dominated footwalls. B) k_{sn} values, showing a similar separation to the mean relief C) HI. More

4.5.1 Relief

The local relief (Fig. 6A) shows a clear divide between faults. The faults which have Proterozoic basement rocks in the footwall (Huoshan, Xizhoushan, Zhongtiaoshan, Hengshan and Wutai) ~~which~~ have a greater range of values ~~and~~ often ~~exceed~~ 400 m. This is especially pronounced for the Wutai and Xizhoushan faults. The Hengshan fault is slightly different as its distribution of relief values is closer to the faults with Palaeozoic-Mesozoic sedimentary rocks in the footwall having most of its values between 200-300m. The Zhongtiaoshan has a maximum at around 200m and therefore lower relief than the other faults but still has some values in the higher ranges with max values of 600m. The faults with Palaeozoic and Mesozoic sedimentary rocks in the footwall (Shilingguan, Taigu, Jiaocheng and Linfen) have overall lower values and a smaller range of values. Most of their values lie between 200-300 m but their minimum values are below 100m. Shilingguan as the RIZ fault shows a similar maximum at 200-300m but is missing the low minimum values resulting in a more compact distribution.

4.5.2 k_{sn}

The ksn value distribution (Fig. 6B) of the different faults shows a similar trend to the Relief as there is generally a good separation between faults with different basement lithology. The faults with Proterozoic basement show much higher values reaching values of 200 while the faults with Palaeozoic-Mesozoic basement show narrower distributions rarely exceeding 100 and most values lying below 50. The notable outliers here are Hengshan which distribution again resembles further the distribution of the Palaeozoic-Mesozoic basement faults. Shilingguan which records much higher values than the other faults with Palaeozoic-Mesozoic basement and has a distribution more similar to the Proterozoic ones.

4.5.2 HI

The HI value distribution (Fig. 6C) differs from the previous two geomorphic indices significantly as the clear separation are not as obvious anymore and the patterns are more dispersed. The general trend still appears that faults with Proterozoic basements have slightly higher values (~0.5), however the Zhongtiaoshan fault while reaching very high HI values has most values sitting at 0.4 which is below the other faults with Proterozoic footwalls and closer to faults with Palaeozoic-Mesozoic sedimentary rocks in the footwall. Within these faults the Linfen and Shilingguan fault show higher values than the other two faults (Taigu and Jiaocheng). Overall, the Shilingguan and Huoshan faults within the RIZs record the highest values but they are not significantly elevated over for example: Wutai or Linfen.

5 Discussion

5.1 Lithology dependence of geomorphic indices

The distribution of geomorphic indices for each fault shows significant differences (Fig. 6). Geomorphic response may be

345 influenced by climate, lithology and tectonics. The climate across Shanxi is continental and shows little variation in precipitation (supplementary material S2) across the study region, which makes the differences in geomorphology between faults unlikely to be controlled by the climate. The lithology in Shanxi is more variable, as seen in Figure 3. The various lithologies can be divided into two main groups that differ in rock strength and erodibility. There are pre-Cambrian rocks which include Archean Tonalite–trondhjemite–granodiorite complexes, high-grade metamorphic rocks and post-orogenic

350 granites which are all part of the TNCO (Trap et al., 2012) and the Palaeozoic-Mesozoic units which include low grade clastic metasediments and carbonates (SBRGM, 1990). Here, we evaluate how these differences in lithology may have impacted the geomorphic response.

Local relief and k_{sn} (Figs. 5A,B) show the highest values where basement lithologies are exposed in the fault footwall. Faults with high mean local relief values (>300m) have "strong" crystalline basement in their footwalls (Huoshan, Wutai,

355 Zhongtiaoshan) or are directly adjacent to these (Xizhoushan), while low values (~<200 m) are found in the faults with Palaeozoic-Mesozoic rocks in their footwalls. HI (Fig. 5c) does not show the same bimodal distribution between faults with different footwall lithologies. The highest HI values correspond to faults with both Proterozoic basement footwall rocks (Huoshan, Wutai, Xizhoushan) and Palaeozoic-Mesozoic footwall rocks (Shilingguan). Meanwhile low values are also found for footwalls of both lithologies (Hengshan, Taigu and Jiaocheng, Zhongtiaoshan). We can infer that the differences in HI

360 values between these fault blocks is not likely to be caused by lithology but rather their tectonic history. This suggests that HI may be a more robust geomorphic index for analysing tectonic activity than relief or k_{sn} because it is less influenced by lithology. Our finding that HI is not primarily influenced by lithology agrees with previous studies (Obaid and Allen, 2019; Groves et al. 2020).

The dependence of some geomorphic indices on lithology is observed in many other areas around the world and highlights

365 the importance of considering the local geology before interpreting the relevance of geomorphic indices (Wobus et al., 2006; Kirby and Whipple, 2012). However, by comparing different faults with similar basement geology the lithological impact can be reduced as theoretically they should have a similar rock strength and erodibility. This enables us to compare the landscape response of these footwall uplifts to tectonics. In the Shanxi Rift, the geomorphic response of faults with relatively "strong" footwall lithology (i.e., crystalline pre-Cambrian basement) such as the Huoshan Fault, shows higher values for

370 geomorphic indices on average compared to faults such as Wutai, Hengshan and Zhongtiaoshan where the footwall lithologies are Proterozoic crystalline basement rocks. The Wutai Fault also has an elevated response compared to the Zhongtiaoshan and the Hengshan faults. Therefore, the difference in geomorphic response between the Huoshan Fault and others in the region cannot be solely attributed to contrasts in lithology. Comparing the response of faults with footwall exposures of Phanerozoic sedimentary rocks it becomes evident that the main bounding fault of the Shilingguan RIZ has a

375 higher geomorphic response than the Jiaocheng, Linfen and Taigu faults. Here the difference in geomorphic response between the Shilingguan RIZ and the other faults is even more pronounced than in the faults with Proterozoic basement in the footwall where the signal is more distributed. It must also be noted that the Shilingguan fault shows a higher HI and ksn value than rocks with "stronger" Proterozoic basement footwalls (Hengshan, Zhongtiaoshan). By comparing faults with similar footwall lithology, we can show that the difference in geomorphic response is not solely ~~down~~ to lithology and most

380 likely has a tectonic origin.

5.2 Implications for rift evolution and linkage

Two significant zones in the evolution of the Shanxi Rift are the two RIZs: Shilingguan and Lingshi that form between the major subbasins. Both zones are generally more elevated than the surrounding basins, making them potential sediment sources (Gawthorpe and Leeder, 1993), which is also shown by their patchy thin sediment fill compared to the major basins

385 (Xu and Ma, 1992), RIZs are classified ~~in~~ their geometrical organisation (underlapping or overlapping, parallel, oblique or orthogonal) and may involve two or more distinct rift segments (Kolawole et al., 2022). The second classification scheme used is their temporal evolution as in are they unbreached, partially breached, recently breached or breached (also Palaeo RIZ) which is assessed mainly based on two metrics: 1) Presence of breaching fault that extends from one rift segment to the other segment and 2) Presence of an established physical linkage of depositional environments of both rift segments (i.e. ~~is~~

390 the drainage between both segments connected). They come with distinct morphological responses and have relevance to the seismic hazard so in the following we will classify the two RIZs based on Kolawole et al. (2022) classification scheme and asses the response of the geomorphic indices.
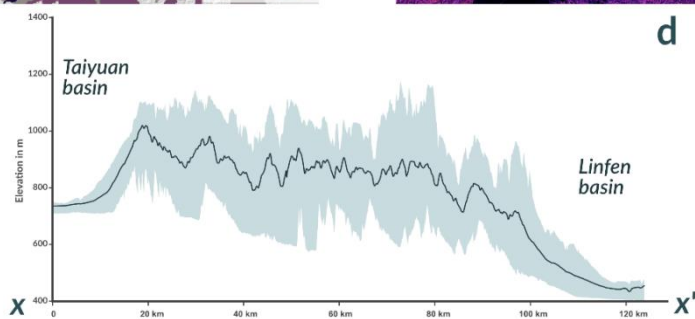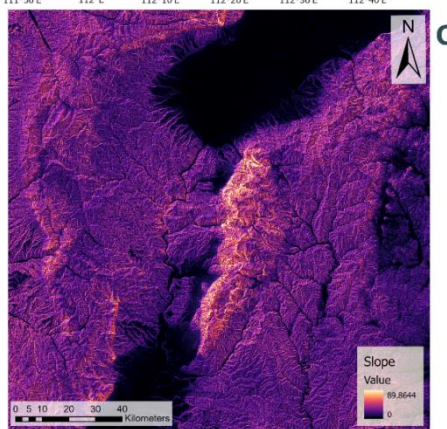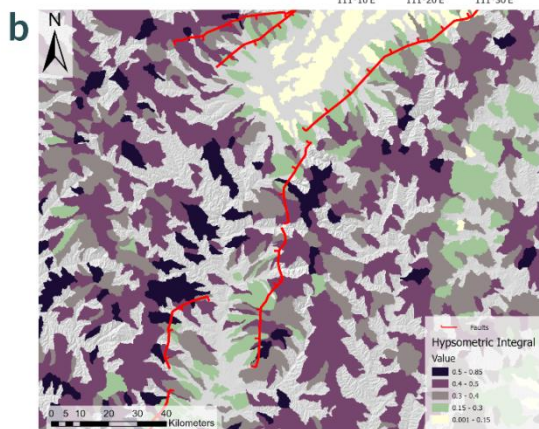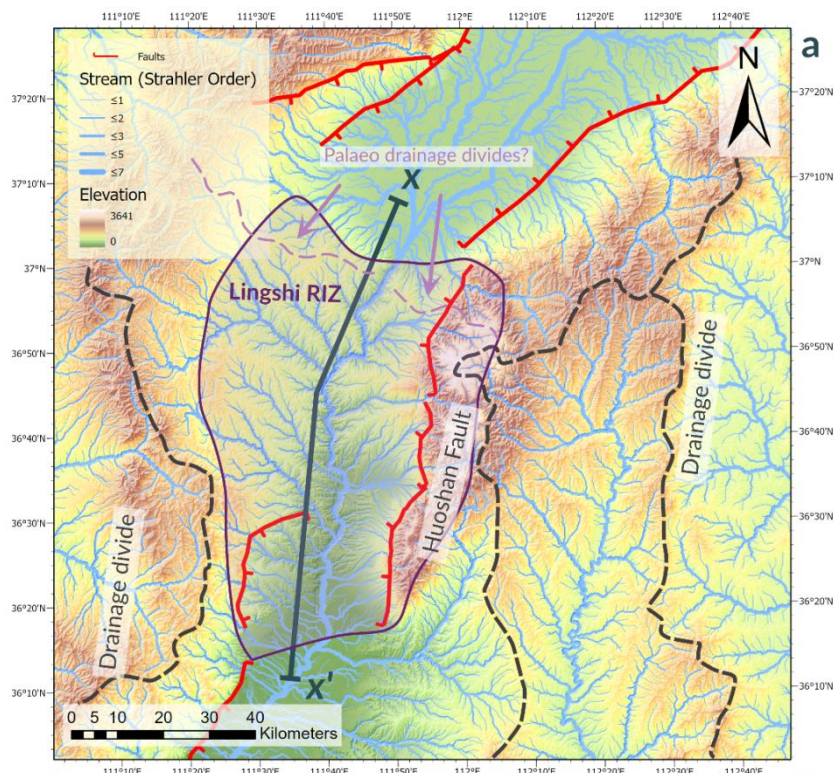
Figure 7: a) Topographic map (based on Shuttle Radar Topography Mission (SRTM) digital elevation model (DEM)) with drainage (weighted by stream order) showing the drainage divide and reorganisation happening at the Lingshi RIZ. b) HI map of the Lingshi RIZ, showing high values in the footwall of the Huoshan Fault but also in the hangingwall. c) Slope map of the Lingshi RIZ that shows very high values along the main border fault (Huoshan) but also clear distinct breaks in the SW. d) S wath profile of the Lingshi RIZ – line of section shown on 7a)

The Lingshi RIZ (Fig. 7) is the southernmost RIZ connecting the Taiyuan and Linfen basins. The breaching fault, which in this case is the Huoshan fault, is well developed and has established a physical connection between the Taiyuan and Linfen basin. The Huoshan fault and other small-scale faults within the Lingshi RIZ are shorter and more segmented than faults of the major subbasins. They also display general a larger variation of orientation. These small-scale faults are more visible in the slope map (Fig. 7c) as sharp linear breaks. The footwall of the Huoshan fault shows high values of HI in the excess of 0.5 (Fig. 7b) however the whole RIZ shows high values of HI which are sometimes connected to smaller scale faults, highlighting the complexity and distribution of faulting in the RIZ. The drainage of the Taiyuan and Linfen basins are connected across the Lingshi RIZ as the Fen River is flowing across it. The drainage was most likely previously not connected as there are possible palaeo-drainage divides (in purple) were tributaries of streams flow in separate directions. Li et al. (1998) proposed that during the early evolution Shanxi Rift in the Miocene and Pliocene the basins were filled by isolated lakes and only during the Mid-Late Pleistocene with renewed tectonic activity the Fen River cut down and established the fluvial connection. Hu et al. (2005) identified three lake terraces in the Taiyuan and Linfen Grabens with the latest regression occurring at 0.13 Ma. Based on this the integration and breaching across the Lingshi RIZ likely occurred in the Late Pleistocene. As the breaching fault (Huoshan) is well developed and established a physical connection between the basins as well as connected the depositional systems of both basins it can be classified as a recently breached RIZ.

The Shilingguan RIZ (Fig. 8) is the RIZ that separates the Xinding basin to the North and the Taiyuan Basin to the South. The breaching fault appears to be physically connected to the Jiaocheng fault but not to the Xizhoushan fault. The footwall of the breaching fault shows very high (>0.5) HI values which is likely connected to recent uplift. The fault itself appears to be segmented as seen by the various orientations of the fault segments (Fig. 8c). The topographic Swath profile of the RIZ shows the topographic highstand of the RIZ (Fig. 8d). The Fen River in the footwall of the Shilingguan bounding fault is highly sinuous but has high topography, relief and steep slopes on either side, also known as an entrenched meander (Gardner, 1975; Harden, 1990). Combined with the high HI responses found in the footwall this shows that this area of the Shanxi Rift has experienced recent uplift. The Shilingguan RIZ represents drainage divide, with the Hutuo River, north of the RIZ is being deflected eastwards and draining across the Xizhoushan fault through the Taihang mountains into the North China Plain. While the Fen River coming from the NW that is crossing the main breaching fault is draining towards the south into the Taiyuan basin. Wind gaps (Fig. 8a) in the footwall of the Xizhoushan to the East show that possibly the drainage of the Fen River once occurred across this RIZ from West to East before uplift and segmentation of the RIZ caused the diversion to the south. As the depositional systems of the Xinding and Taiyuan basin are not connected across the RIZ and the breaching fault has not established a full physical link, this RIZ most likely represents a partially breached RIZ.
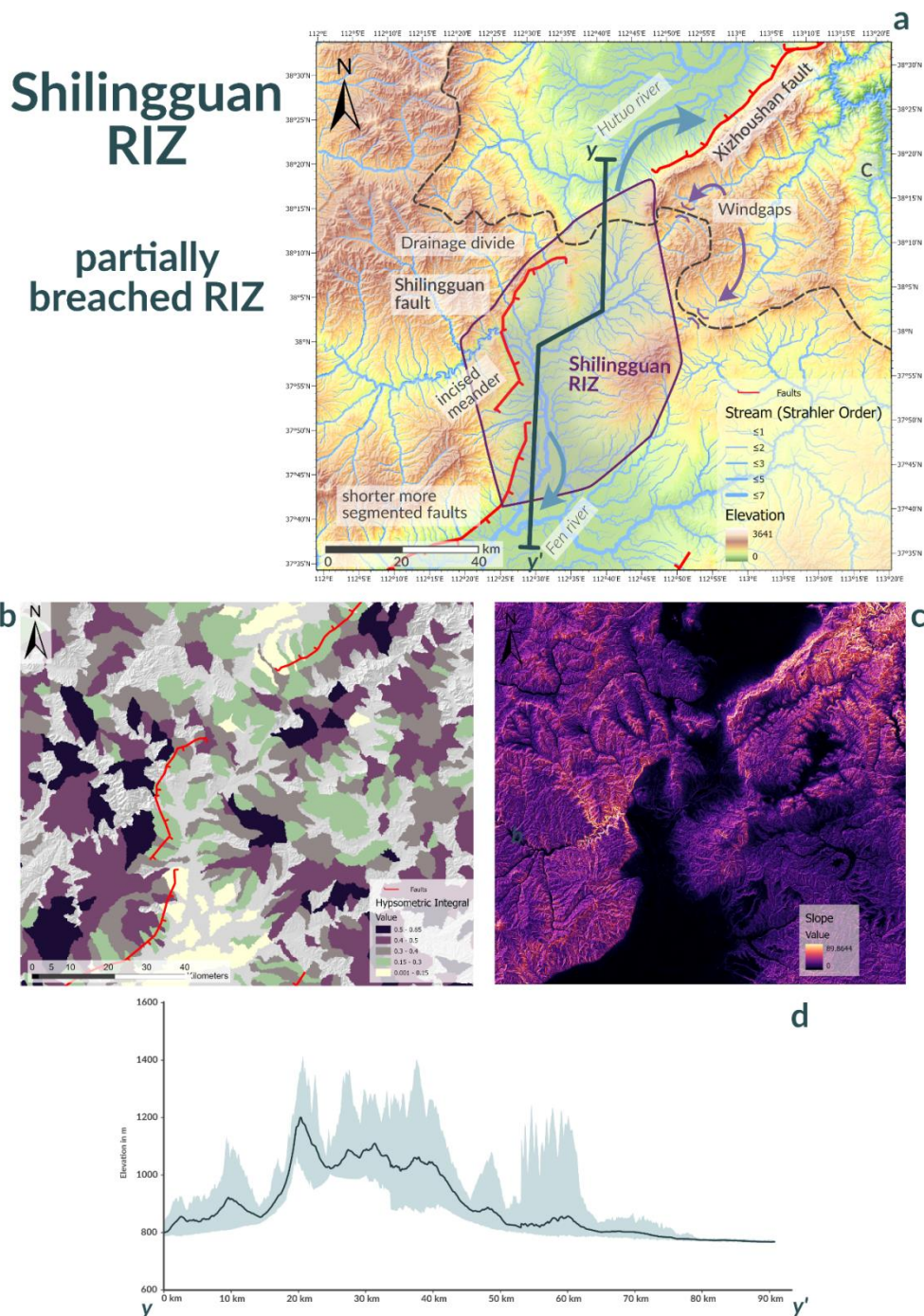
Figure 8: a) Topographic map (based on Shuttle Radar Topography Mission (SRTM)-digital elevation model (DEM)) with streams (weighted by stream order) showing the drainage divide and reorganisation happening at the Shilingguan RIZ. b) HI map of the Shilingguan RIZ, showing the high values in the footwall of the main faults, especially in the Shilingguan fault footwall where the high slope values are found. c) Slope map of the Shilingguan RIZ. High slope values are closely associated with the main faults but

435 **can also be seen along the steep sides of the meandering rivers in both the footwall of the Xizhoushan Fault and the Shilingguan Fault. d) Swath profile of the Shilingguan RIZ – line of section shown in 8a)**

Geomorphic evidence shows that the RIZ are currently the most active regions of faulting and reorganisation, they also show major changes in fault strike compared to the NE-SW trending basins. Most faults in the RIZs do not strike NE-SW, as ~~is the case for the major basin bounding faults but~~ show more distributed patterns of N-S and NE-SW striking faults. Commonly,

440 an overall "zig-zag pattern" forms, with fault segments of variable direction. Faults oblique to the general extension direction commonly form at the intersection points between major faults. Hodge et al. (2018a) show in models that Coulomb stress changes along the tips of established faults lead to the formation of new off-axis trending faults, with the geometry of these dependent on separation and amount of under- or overlap of the rift segments. This process is common in other rift basins across the world (Maerten et al., 2000; Morley, 2017) and is similar to observations of faults in the RIZs of the Shanxi Rift.

445 The NS striking fault segments in the RIZs show overall higher geomorphic index values compared to the NE-SW trending faults of the sub-basins, suggesting they are more tectonically active as the active deformation is focused along zones of active linkage. The morphology of the NS faults in the RIZs suggest that they are likely younger faults which are still early in the reorganisation phase, as they are shorter, more segmented and show ~~often~~ lower topographic offset. ~~While the~~ morphologically more mature NE-SW striking basin bounding faults generally have lower geomorphic index values than the

450 faults in the RIZs~~, they~~ also ~~can~~ show high values, especially in the case of the Wutai and Xizhoushan faults. This pattern shows ~~how complex the~~ activity pattern in the Shanxi ~~is~~, as faults of all orientations may show high activity levels, ~~however~~ faults in the RIZs show ~~relatively~~ the highest activity. This is consistent with the idea of an overall stable extension direction where all faults remain ~~possibly~~ active but activity is concentrated in the linkage zones.

RIZs often experience increased seismic activity due to the higher fault activity along the tips of the surrounding basements

455 linking through into through going zones. Increased strain rate on faults post linkage has been shown to occur both in theory (Cowie et al. 2005) and ~~praxis, for example in~~ the Whakatne Graben, NZ (Taylor, 2004). The heightened activity at these RIZs is not only shown by geomorphology but also ~~in~~ seismicity: Chen et al. (2021) processed receiver function data that shows cluster of earthquakes at or near both above-mentioned RIZs while events in the individual subbasins ~~is~~ more distributed. The ICS catalogue (Storchak et al., 2013, 2015; Di Giacomo et al., 2018) covering earthquakes occurring

460 between 1907 and 2022 (Supplementary Material S3) show similar clusters around the RIZ, although the cluster around the Shilingguan RIZ is arguably more pronounced. While the faults in the Shilingguan RIZ are comparatively short and segmented (10-20km) which might limit their ability to generate large magnitude earthquakes, the Huoshan Piedmont Fault in the Lingshi RIZ is associated with the historic Hongdong Earthquake of ~~CE~~ 1303, which was an *M*w 7.2-7.6 event (Xu et al., 2018), it has a an estimated rupture length of 98km which show ~~the~~ multiple segments can link up during seismic slip to

465 generate larger magnitude events. The Shanxi Rift is a low strain rate region, meaning major earthquakes are infrequent but potentially devastating as evidenced by the Hongdong 1303 event (Xu et al., 2018). The breaching faults in the RIZ could have a buffering effect on the NE-SW trending faults of the main sub-basins, as they concentrate the overall strain

accommodated across the Shanxi Graben. Overall, the NE-SW trending faults which are longer but potentially less active might be capable of generating larger but more infrequent events (Scholz et al., 1982), while the more segmented faults in the

470   RIZs could produce more frequent yet smaller magnitude earthquakes.

5.3 The role of inheritance in the Shanxi Rift – crust or mantle control?

Most continental rifts are influenced by inherited structures that are either reactivated (Holdsworth et al., 2001) or reorientate the stresses (Morley, 2010; Samsu et al. in review). At a first order scale the relationship of the Shanxi Rift and the TNCO is obvious (Fig. 1). The Shanxi Rift system is almost directly superimposed on the Paleoproterozoic orogen (Xu and Ma,

475   1993). The TNCO acted most likely as a rheological weakness in comparison to the adjacent stronger Western Block of the NCC, which was exploited by the Shanxi Rift. Orogenic belts behaving as weak zones for nucleating rifts is common (i.e. East Africa –(Rosendahl, 1987, Morley, 1988, Ring, 1994) or Baikal (Petit et al., 1996). Faults define the edges of Paleoproterozoic basement complexes and expose these at the surface. While some faults do not directly expose Precambrian rocks in the footwall, such as the Jiaocheng or Taigu faults, they form near Precambrian basement complexes such as the

480   Lüliangshan or the Taihangshan (less than 50km away in the case of the Jiaocheng and the Lüliangshan). It is likely that Shanxi Rift border faults exposed these rocks to the surface through footwall uplift. Basement complexes such as the Huoshan, Fuping or Lüliangshan are also cored by Precambrian granitic plutons, which formed as late orogenic intrusions during the orogeny that formed the TNCO. These stronger, more buoyant granitic blocks may have been more resistant to deformation, and faults formed around them uplifting at the core of the footwalls similar to observations offshore New

485   Zealand (Phillips and McCaffrey, 2019) or Carboniferous rift systems of the United Kingdom (Fraser and Gawthorpe, 1990; Howell et al., 2020). The Shanxi Rift most likely exploited rheological weaknesses during its formation on large rift system scale and on smaller individual fault scales.
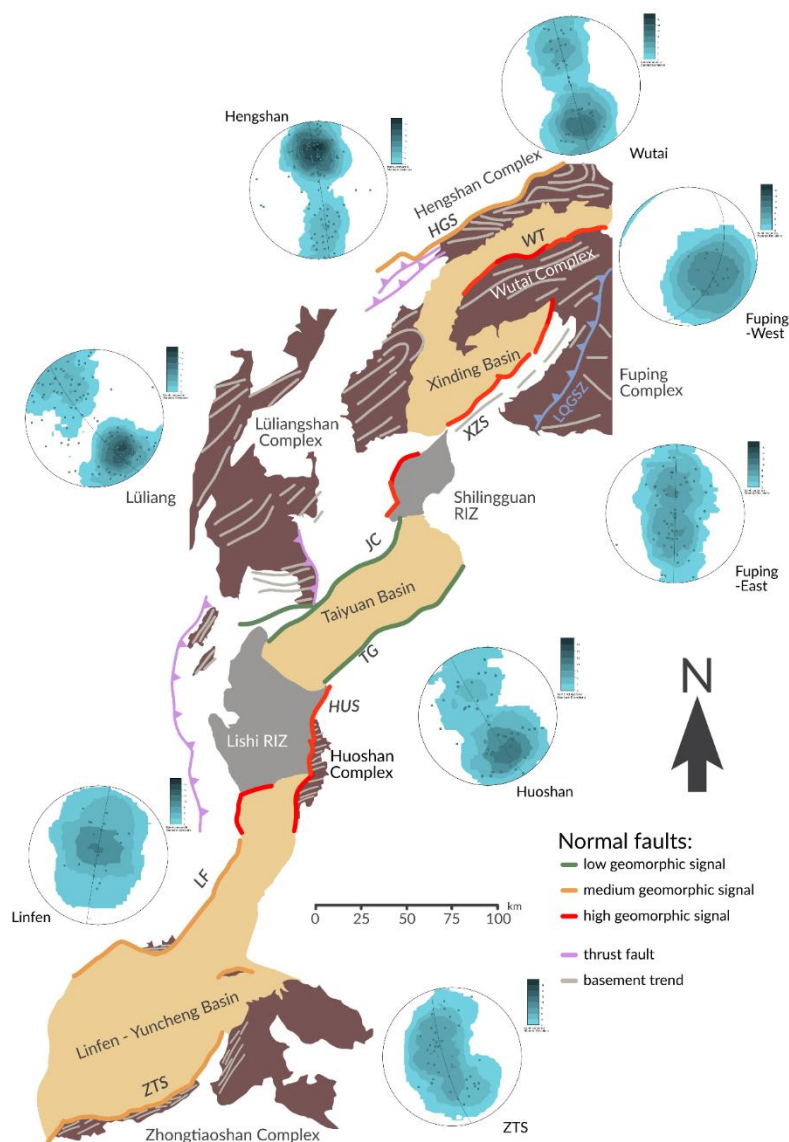
Figure 9: Schematised fault map of the Shanxi Rift with faults colour coded according to their geomorphic signal. Outcropping
490   **basement of the TNCO in brown with the main structural trends highlighted in light grey. The poles to planes stereonets (data from Trap et al., 2007; Trap et al., 2009a) show the structural grain of the main basement complexes. Most basement complexes show a NE-SW orientated grain, but it is more E-W in the North.**

Major NE-SW trending basin bounding faults in the Shanxi Rift (Wuati, Xizhoushan, Taigu, Jiaocheng, Zhongtiaoshan) are
495   generally parallel to inherited NE-SW (45-55°) trending Paleoproterozoic basement fabrics (Fig. 9). The Wutai, Zhongtiaoshan and Hengshan faults all strike ~~more~~ ENE-WSW (60-70°) ~~than the other faults~~, matching the trend of the inherited structures in the footwall of these faults, therefore it is likely that crustal structures ~~altered~~ the orientation of these

faults. The Xizhoushan fault mainly follows the trend of the fabrics in the western part of the Fuping complex. There is a major crustal boundary running through the Fuping complex which is known as the Longquanguang Shear Zone (LGQSZ)
500 which is according to Trap et al. (2012) a gently dipping ductile thrust fault. To the Southeast of the LGQSZ there is a major change in trend of the Palaeoproterozoic fabrics to a generally NW-SE/E-W direction (compare Stereonets Fuping-West and East on Fig. 9). The crustal structures of the eastern Fuping Block appear to have no influence on the Xizhoushan fault (or any other fault in the Shanxi Rift), possibly because the LGQSZ represents a barrier. The Xizhoushan fault may merge with the LQGSZ at depth, however, this is mostly speculative based on their matching orientation and proximity. Merging of
505 faults on shallower dipping structures has been observed by Phillips et al. (2016) in the North Sea. The similar trends of ancient pre-existing structures and active extensional faults show that the Paleoproterozoic fabrics of the TNCO potentially influence the orientation and morphology of the active faults of the Shanxi Graben.

Faults in the RIZs show a more segmented pattern (Figs. 7, 8), vary more in orientation (N-S and NE-SW) and are shorter (10-30 km) than the large NE-SW trending basin bounding faults (up to 100 km). Individual fault segments in the RIZs
510 alternate between following the crustal inherited fabric which broadly trends NE-SW, or cutting across the fabric and striking more N-S or NNE-SSW. As faults mature, segments link up and grow into one through going structure that has a "zig-zag" pattern that cuts across pre-existing fabrics; this is especially visible on plan-view of the Huoshan Piedmont Fault (Fig. 7). These "zig-zag" patterns in faults have been observed in various other rifts such as offshore West Greenland (Peace et al. 2018, Schiffer et al. 2020), the North Sea (Henstra et al., 2015) and the main Ethiopian Rift (Moore and Davidson, 1978;
515 Vetel and Le Gall, 2006; Corti et al., 2022). In the case of Greenland and Ethiopia, rifting was oblique to major basement shear zones which lead to the formation of three sets of faults with some of them roughly parallel to the extension direction and others parallel to the inherited structures. In the Shanxi Rift the regional strain field around the RIZs is likely perturbated due to interactions of the fault tips of the adjacent basin-bounding faults. The strain field would be oblique to the inherited structures, thus resulting in N-S trending faults perpendicular to the proposed perturbated strain field and NE-SW trending
520 faults following the trend of pre-existing Proterozoic structures. Therefore, as the faults grow and coalesce across the RIZs they will both cut across or locally exploit the inherited fabrics. Fault geometry may also be controlled by multiple levels of inheritance as observed by Wedmore et al. (2020) for the Thyolo Fault in Malawi and Hodge et al. (2018b) for the Bilila-Mtakataka Fault, where shallow level structures control surface geometry of the fault but a deeper-seated weakness controls the overall orientation which is oblique to the overall strain field. Another possibility is that the NE-SW trending faults in the
525 RIZs formed parallel to inherited fabrics early and later were linked up by N-S trending segments. This behaviour was observed on the Norwegian Margin of the North Sea by Henstra et al. (2015) where early rift faults from a E-W orientated phase of rifting influenced the location and morphology of later rift faults during a subsequent phase of rifting, which was orientated obliquely to the early faults. However, we did not find major morphological or geomorphological value differences between the N-S and NE-SW trending faults that would suggest that one set formed earlier, therefore it is more
530 likely that they are co-eval. In summary, crustal inherited fabrics are a major factor in the segmentation and reorientation of the "zig-zag faults" found in the RIZs.
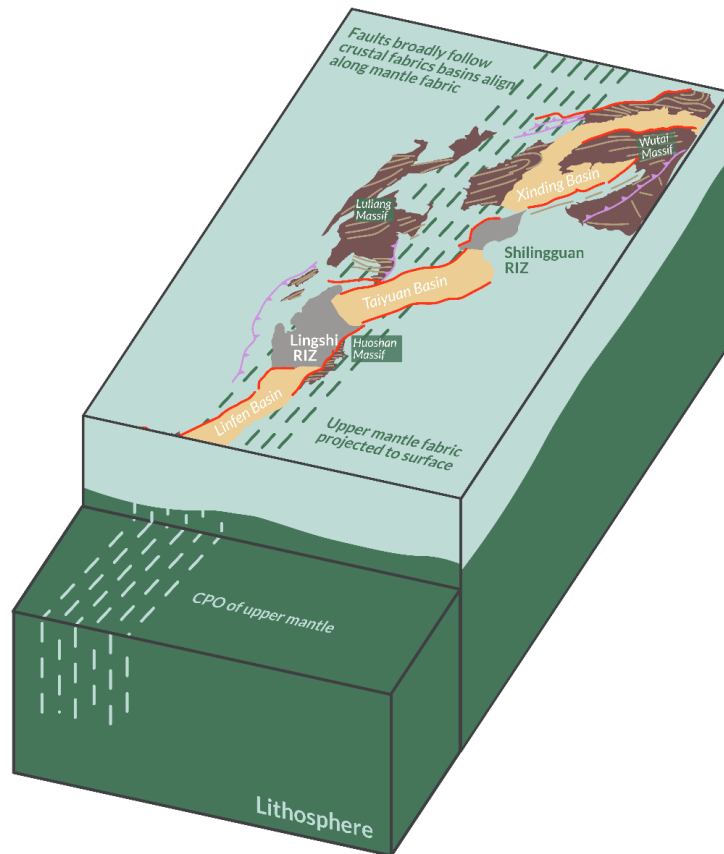
Figure 10: Schematic 3D diagram of the Shanxi Rift showing the proposed obliquity between mantle anisotropy and crustal inherited fabrics. Mantle anisotropy is defined by the suggested crystal preferred orientation (evidenced by shear wave splitting data (Zhao and Zheng, 2005)) in the upper mantle, that broadly trends N-S, while the crustal fabrics trend NE-SW. The Shanxi Rift basins align along surface projection of the mantle anisotropy which is oblique to the principal extension direction. Individual basins and their bounding faults formed parallel to inherited crustal fabrics. This creates the characteristic en-echelon pattern of the Shanxi Rift.

540 The N-S and NE-SW trends of faults found at local scale in the RIZs are ~~can~~ also be observed for the entire Shanxi Rift ~~system~~. The Shanxi Rift is an S-shaped en-echelon rift that follows a broad N-S trend, with individual basins and their bounding-faults orientated NE-SW. While the TNCO broadly trends N-S or NNE-SSW (Fig. 1; Zhao et al., 2005), the individual crustal structures such as major shear zones, thrust faults or fabrics broadly trend NE-SW (Fig. 10). A broadly NNE-SSW to N-S trending anisotropy (0-15°) in the upper mantle of the Central Zone of the North China Craton is shown

545 by shear wave splitting data from the upper mantle (Chen et al., 2010; Zhao and Zheng, 2005). This shows that crustal inheritance and the lithospheric inheritance may not share a common orientation, which is a common feature of many rift zones (Vauchez et al., 1997; Tomassi and Vauchez, 2001). Recent analogue modelling of oblique crustal and mantle fabrics by Zwaan et al. (2022) show similar patterns to those observed in Shanxi. Numerical modelling by Molnar et al. (2020) show

that lithospheric weaknesses influence the rift trend while oblique crustal structures segment the rift at a local scale. The

550 difference in lithospheric and crustal structural trend could have either occurred during transpressional accretion of the Trans-North China Orogen or during later reworking by the polyorogenic event that formed the Trans-North China Orogen, such as has been proposed by Kusky and Li (2003) Mesozoic compression across North China, commonly known as the Yanshanian orogeny (Zhang et al. 2007; Clinkscales and Kapp, 2019) has also effected the Shanxi region and may have also caused further reworking of the TNCO and rotated to the crustal fabrics to the present day orientation. Determining the exact

555 reason for the apparent offset between crustal and lithospheric trends of the TNCO is not resolvable in this study and would require further work. The principal extension direction determined by Middleton et al. (2017) of 151° for the Shanxi Rift is roughly perpendicular to the inherited structures in the crust but oblique to the proposed broad upper mantle anisotropy, which resulted in the early rift basins exploiting the favourably orientated crustal fabrics while the general trend of the rift is oblique to the extension direction along an upper mantle fabric that created a rheological weakness.

560 We propose a new model for the evolution of the Shanxi Rift that incorporates a heterogenous basement with inherited structures. This model is consistent with our geomorphic results (Fig.11) can explain the evolution of the Shanxi Rift System under a constant strain field making it simpler than the frequent changes in the strain field that have been proposed by others (Shi et al., 2015a; Shi et al., 2020; Assie et al., 2022). In our model the extensional strain field trends roughly NW-SE which is consistent with previous estimations of the present-day extensional strain field using GPS or seismicity data (Middleton et

565 al., 2017; Shen et al., 2000). However locally the strain is reorientated either by inherited structures (I.e., Wutai and Hengshan) or interactions between faults that rotate the local strain field in the interaction zone between them (Shilingguan and Huoshan) This means that there is no specific set of faults that is favoured by changes of strain fields therefore potentially all faults remain active. There are certain faults that are more active either due to the influence of inherited structures or active reorganisation and linkage in RIZs. Faults established early on along preferentially aligned NE-SW

570 trending inherited structures and formed the major basins: Taiyuan, Xinding and Linfen. These basins formed en-echelon along an oblique trending upper mantle structure. As the faults and basins grew, they started interacting and linking across topographical highstands that saw less faulting and subsidence — the RIZs. These have a more complex faulting pattern as the interacting faults create a local rotated strain field which is oblique to the crustal structures. This creates a "zig-zag geometry" as the smaller more segmented fault segments grow and coalesce. As linkage progresses these RIZs link the

575 different basins and establish physical and sedimentary system links. Which is the current present-day phase.

Fig. 11. The new proposed evolutionary model under a constant strain field that shows linkage of rift basins influenced by two levels of inheritance – crustal and mantle inheritance, which result in oblique rifting and the creation of en-echelon array of basins. Crustal fabrics aid strain accommodation and influence geometry of linkage faults in the RIZs.

6 Conclusions

Geomorphic indices are a powerful tool to evaluate the evolution and segmentation of the Shanxi Rift. Our study shows that lithology has a strong influence on the overall geomorphic signal of faults, as those with Paleoproterozoic crystalline basement in their footwalls have an overall higher geomorphic value compared to faults with Palaeozoic-Mesozoic metasediments in the footwalls. However, comparing faults with similar basement geology can circumvent this problem. We found that overall HI is less sensitive to these variations of lithology compared to Relief and k_{sn}. Therefore, HI may be more suited to evaluating the tectonic influence on landscapes.

The geomorphic analysis showed that in the Shanxi Rift the RIZs that link the established large basins, namely the Xinding and Taiyuan basins, are the most active zones and show most signs of active drainage reorganisation. Linkage of the sub-basins seems to be progressing towards the North. This has major implications for seismic hazard assessments as it hints

590 towards zones which show more complex and more active patterns of faulting which might be the site of future major earthquakes.

Structural Inheritance played a key role in the evolution and segmentation of the Shanxi Rift. The collision of the ~~two~~ blocks of the NCC created a lithospheric scale weak zone -the Trans North China Orogen-- which preferentially accommodates strain as it is more easily deformed than the surrounding cratonic area. The individual sub-basins of the Shanxi Rift ~~system~~

595 align along a broad NNE-SSW trend which coincides with an upper mantle anisotropy fabric – a lithospheric manifestation of the TNCO. Inherited fabrics in the upper crust are orientated NE-SW, perpendicular to the regional extension direction. The extension direction is oblique to the assumed upper mantle inherited fabric which causes the en-echelon pattern of individual rift basins. Early rift faults nucleated ~~in zones of preferentially (NE-SW) aligned~~ basement fabrics establishing basins separated by NS trending RIZs. Within these RIZs the ~~crustal basement~~ inheritance further influenced and segmented

600 the breaching faults and aided linkage across the basins. The faults within ~~them~~ both follow and crosscut pre-existing fabrics in the crust creating a "zig-zag pattern" of small, segmented faults that eventually link up into ~~singular~~ throughgoing fault zones. Therefore, structural inheritance of pre-existing Precambrian basement fabrics as well as large scale early established faults interacted to perturbate the strain field ~~and~~ created a 3D strain field resulting in the complex pattern of faulting we now see in the RIZs. Thus, frequent changes of the strain field are not needed to explain the evolution of the Shanxi Rift as data is

605 consistent with an evolution under a constant strain field.

We propose that the Shanxi Rift is a type-example of an oblique rift that is influenced by ~~an~~ inheritance at different scales, as upper mantle and crustal basement structures as well as ~~pre-existing~~ faults have influenced the pattern of faulting observed today.

References

610 Agostini, A., Bonini, M., Corti, G., Sani, F., Mazzarini, F., 2011. Fault architecture in the Main Ethiopian Rift and comparison with experimental models: Implications for rift evolution and Nubia–Somalia kinematics. Earth and Planetary Science Letters 301, 479–492. https://doi.org/10.1016/j.epsl.2010.11.024

Ahnert, F., 1970. Functional relationships between denudation, relief, and uplift in large, mid-latitude drainage basins. American Journal of Science 268, 243–263. https://doi.org/10.2475/ajs.268.3.243

615 Ai, S., Zheng, Y., He, L., Song, M., 2019. Joint inversion of ambient noise and earthquake data in the Trans-North China Orogen: On-going lithospheric modification and its impact on the Cenozoic continental rifting. Tectonophysics 763, 73–85. https://doi.org/10.1016/j.tecto.2019.05.003

Allen, M. B., Macdonald, D.I.M., Xun, Z., Vincent, S.J., Brouet-Menzies, C., 1997. Early Cenozoic two-phase extension and late Cenozoic thermal subsidence and inversion of the Bohai Basin, northern China. Marine and Petroleum Geology 14,

620 951–972. https://doi.org/10.1016/S0264-8172(97)00027-5

Allen, M.B., Macdonald, D.I.M., Xun, Z., Vincent, S.J., Brouet-Menzies, C., 1997. Early Cenozoic two-phase extension and late Cenozoic thermal subsidence and inversion of the Bohai Basin, northern China. Marine and Petroleum Geology 14, 951–972. https://doi.org/10.1016/S0264-8172(97)00027-5

Assie, K.R., Wang, Y., Tranos, M.D., Ma, H., Kouamelan, K.S., Brantson, E.T., Zhou, L., Ketchaya, Y.B., 2022. Late
625   Cenozoic faulting deformation of the Fanshi Basin (northern Shanxi rift, China), inferred from palaeostress analysis of mesoscale fault-slip data. Geological Magazine 1–17. https://doi.org/10.1017/S0016756822000085

Boccaletti, M., Mazzuoli, R., Bonini, M., Trua, T., Abebe, B., 1999. Plio-Quaternary volcanotectonic activity in the northern sector of the Main Ethiopian Rift: relationships with oblique rifting. Journal of African Earth Sciences 29, 679–698. https://doi.org/10.1016/S0899-5362(99)00124-4

630   Bonini, M., Souriot, T., Boccaletti, M., Brun, J.P., 1997. Successive orthogonal and oblique extension episodes in a rift zone: Laboratory experiments with application to the Ethiopian Rift. Tectonics 16, 347–362. https://doi.org/10.1029/96TC03935

Brune, S., Corti, G., Ranalli, G., 2017. Controls of inherited lithospheric heterogeneity on rift linkage: Numerical and analog models of interaction between the Kenyan and Ethiopian rifts across the Turkana depression. Tectonics 36, 1767–1786. https://doi.org/10.1002/2017TC004739

635   Brune, S., Williams, S.E., Müller, R.D., 2018. Oblique rifting: the rule, not the exception. Solid Earth 9, 1187–1206. https://doi.org/10.5194/se-9-1187-2018

C. K. Morley, R. a. N., Munn, S.G., 1990. Transfer Zones in the East African Rift System and Their Relevance to Hydrocarbon Exploration in Rifts (1). AAPG Bulletin 74, 1234–1253.

Chen, G., 1987. On the geotectonic nature of the Fen-Wei rift system. Tectonophysics, Continental Rifts-Principal and
640   Regional Characteristics 143, 217–223. https://doi.org/10.1016/0040-1951(87)90091-6

Chen, L., 2010. Concordant structural variations from the surface to the base of the upper mantle in the North China Craton and its tectonic implications. Lithos, The lithosphere/asthenosphere boundary: Nature, formation and evolution 120, 96–115. https://doi.org/10.1016/j.lithos.2009.12.007

Chen, T., Zhang, P.Z., Liu, J., Li, C.Y., Ren, Z.K., Hudnut, K.W., 2014. Quantitative study of tectonic geomorphology along
645   Haiyuan fault based on airborne LiDAR. Chin. Sci. Bull. 59, 2396–2409. https://doi.org/10.1007/s11434-014-0199-4

Chen, W.-P., Nábelek, J., 1988. Seismogenic strike-slip faulting and the development of the North China Basin. Tectonics 7, 975–989. https://doi.org/10.1029/TC007i005p00975

Chen, Y., Chen, J., Li, S., Yu, Z., Liu, X., Shen, X., 2021. Variations of crustal thickness and average Vp/Vs ratio beneath the Shanxi Rift, North China, from receiver functions. Earth, Planets and Space 73, 200. https://doi.org/10.1186/s40623-021-
650   01528-8

Clemson, J., Cartwright, J., Booth, J., 1997. Structural segmentation and the influence of basement structure on the Namibian passive margin. Journal of the Geological Society 154, 477–482.

Clinkscales, C., Kapp, P., 2019. Structural style and kinematics of the Taihang-Luliangshan fold belt, North China: Implications for the Yanshanian orogeny. Lithosphere 11, 767–783. https://doi.org/10.1130/L1096.1

655   Clinkscales, C., Kapp, P., Thomson, S., Wang, H., Laskowski, A., Orme, D.A., Pullen, A., 2021. Regional exhumation and
        tectonic history of the Shanxi Rift and Taihangshan, North China. Tectonics 40, e2020TC006416.

        Corti, G., 2009. Continental rift evolution: From rift initiation to incipient break-up in the Main Ethiopian Rift, East Africa.
        Earth-Science Reviews 96, 1–53. https://doi.org/10.1016/j.earscirev.2009.06.005

        Corti, G., 2008. Control of rift obliquity on the evolution and segmentation of the main Ethiopian rift. Nature Geosci 1, 258–
660   262. https://doi.org/10.1038/ngeo160

        Corti, G., Iandelli, I., Cerca, M., 2013. Experimental modeling of rifting at craton margins. Geosphere 9, 138–154.
        https://doi.org/10.1130/GES00863.1

        Corti, G., Maestrelli, D., Sani, F., 2022. Large-to Local-Scale Control of Pre-Existing Structures on Continental Rifting:
        Examples From the Main Ethiopian Rift, East Africa. Frontiers in Earth Science 10.

665   Cowie, P.A., Underhill, J.R., Behn, M.D., Lin, J., Gill, C.E., 2005. Spatio-temporal evolution of strain accumulation derived
        from multi-scale observations of Late Jurassic rifting in the northern North Sea: A critical test of models for lithospheric
        extension. Earth and Planetary Science Letters 234, 401–419. https://doi.org/10.1016/j.epsl.2005.01.039

        Cox, R.T., 1994. Analysis of drainage-basin symmetry as a rapid technique to identify areas of possible Quaternary tilt-block
        tectonics: An example from the Mississippi Embayment. GSA Bulletin 106, 571–581. https://doi.org/10.1130/0016-
670   7606(1994)106<0571:AODBSA>2.3.CO;2

        Crider, J.G., Pollard, D.D., 1998. Fault linkage: Three-dimensional mechanical interaction between echelon normal faults.
        Journal of Geophysical Research: Solid Earth 103, 24373–24391. https://doi.org/10.1029/98JB01353

        Davis, G., Zheng, Y., Cong, W., Darby, B., Zhang, C., Gehrels, G., 2001. Mesozoic tectonic evolution of the Yanshan fold
        and thrust belt, with emphasis on Hebei and Liaoning provinces, northern China, in: Geol. Soc. Am. Mem. pp. 171–197.
675   https://doi.org/10.1130/0-8137-1194-0.171

        Deng, Q., Ran, Y., Yang, X., Min, W., Chu, Q., 2007. Map of Active tectonics in China, Seismological Press

        Densmore, A.L., Dawers, N.H., Gupta, S., Allen, P.A., Gilpin, R., 2003. Landscape evolution at extensional relay zones.
        Journal of Geophysical Research: Solid Earth 108. https://doi.org/10.1029/2001JB001741

        Densmore, A.L., Dawers, N.H., Gupta, S., Guidon, R., Goldin, T., 2004. Footwall topographic development during
680   continental extension. Journal of Geophysical Research: Earth Surface 109. https://doi.org/10.1029/2003JF000115

        Densmore, A.L., Gupta, S., Allen, P.A., Dawers, N.H., 2007. Transient landscapes at fault tips. Journal of Geophysical
        Research: Earth Surface 112. https://doi.org/10.1029/2006JF000560

        DiBiase, R.A., Whipple, K.X., Heimsath, A.M., Ouimet, W.B., 2010. Landscape form and millennial erosion rates in the San
        Gabriel Mountains, CA. Earth and Planetary Science Letters 289, 134–144. https://doi.org/10.1016/j.epsl.2009.10.036

685   Di Giacomo, D., E.R. Engdahl and D.A. Storchak (2018). The ISC-GEM Earthquake Catalogue (1904–2014): status after the
        Extension Project, Earth Syst. Sci. Data, 10, 1877-1899, doi: 10.5194/essd-10-1877-2018.

        Dong, S., Zhang, Y., Zhang, F., Cui, J., Chen, X., Zhang, S., Miao, L., Li, J., Shi, W., Li, Z., Huang, S., Li, H., 2015. Late
        Jurassic–Early Cretaceous continental convergence and intracontinental orogenesis in East Asia: A synthesis of the Yanshan

Revolution. Journal of Asian Earth Sciences, Mesozoic Lithospheric Structures and Tectonic Development of East Asia 114,
690   750–770. https://doi.org/10.1016/j.jseaes.2015.08.011

Dulanya, Z., Gallen, S.F., Kolawole, F., Williams, J.N., Wedmore, L.N.J., Biggs, J., Fagereng, Å., 2022. Knickpoint
morphotectonics of the Middle Shire River basin: Implications for the evolution of rift interaction zones. Basin Research 34,
1839–1858. https://doi.org/10.1111/bre.12687

Dunbar, J.A., Sawyer, D.S., 1988. Continental rifting at pre-existing lithospheric weaknesses. Nature 333, 450–452.
695   https://doi.org/10.1038/333450a0

Ebinger, C.J., Rosendahl, B.R., Reynolds, D.J., 1987. Tectonic model of the Malaŵi rift, Africa. Tectonophysics,
Sedimentary basins within the Dead Sea and other rift zones 141, 215–235. https://doi.org/10.1016/0040-1951(87)90187-9

Erbello, A., Melnick, D., Zeilinger, G., Bookhagen, B., Pingel, H., Strecker, M.R., 2022. Geomorphic expression of a
tectonically active rift-transfer zone in southern Ethiopia. Geomorphology 403, 108162.
700   https://doi.org/10.1016/j.geomorph.2022.108162

Faulds, J.E., Varga, R.J., 1998. The role of accommodation zones and transfer zones in the regional segmentation of
extended terranes, in: Faulds, J.E., Stewart, J.H. (Eds.), Accommodation Zones and Transfer Zones; the Regional
Segmentation of the Basin and Range Province. Geological Society of America, p. 0. https://doi.org/10.1130/0-8137-2323-
X.1

705   Faure, M., Trap, P., Lin, W., Monié, P., Bruguier, O., 2007. Polyorogenic evolution of the Paleoproterozoic Trans-North
China Belt—New insights from the Lüliangshan-Hengshan-Wutaishan and Fuping massifs. Episodes Journal of International
Geoscience 30, 96–107.

Fazlikhani, H., Fossen, H., Gawthorpe, R.L., Faleide, J.I., Bell, R.E., 2017. Basement structure and its influence on the
structural configuration of the northern North Sea rift. Tectonics 36, 1151–1177. https://doi.org/10.1002/2017TC004514

710   Flint, J.-J., 1974. Stream gradient as a function of order, magnitude, and discharge. Water Resources Research 10, 969–973.

Fossen, H., Rotevatn, A., 2016. Fault linkage and relay structures in extensional settings—A review. Earth-Science Reviews
154, 14–28. https://doi.org/10.1016/j.earscirev.2015.11.014

Fraser, A.J., Gawthorpe, R.L., 1990. Tectono-stratigraphic development and hydrocarbon habitat of the Carboniferous in
northern England. Geological Society, London, Special Publications 55, 49–86.
715   https://doi.org/10.1144/GSL.SP.1990.055.01.03

Gao, M., Zeilinger, G., Xu, X., Tan, X., Wang, Q., Hao, M., 2016. Active tectonics evaluation from geomorphic indices for
the central and the southern Longmenshan range on the Eastern Tibetan Plateau, China. Tectonics 35, 1812–1826.
https://doi.org/10.1002/2015TC004080

Gao, S., Rudnick, R.L., Carlson, R.W., McDonough, W.F., Liu, Y.-S., 2002. Re–Os evidence for replacement of ancient
720   mantle lithosphere beneath the North China craton. Earth and Planetary Science Letters 198, 307–322.
https://doi.org/10.1016/S0012-821X(02)00489-2

Gao, S., Rudnick, R.L., Yuan, H.-L., Liu, X.-M., Liu, Y.-S., Xu, W.-L., Ling, W.-L., Ayers, J., Wang, X.-C., Wang, Q.-H., 2004. Recycling lower continental crust in the North China craton. Nature 432, 892–897. https://doi.org/10.1038/nature03162

725   Gardner, T.W., 1975. The History of Part of the Colorado River and Its Tributaries: An Experimental Study 87–95.

Gawthorpe, R.L., Hurst, J.M., 1993. Transfer zones in extensional basins: their structural style and influence on drainage development and stratigraphy. Journal of the Geological Society 150, 1137–1152. https://doi.org/10.1144/gsjgs.150.6.1137

Geurts, A.H., Cowie, P.A., Duclaux, G., Gawthorpe, R.L., Huismans, R.S., Pedersen, V.K., Wedmore, L.N.J., 2018. Drainage integration and sediment dispersal in active continental rifts: A numerical modelling study of the central Italian

730   Apennines. Basin Research 30, 965–989. https://doi.org/10.1111/bre.12289

Geurts, A.H., Whittaker, A.C., Gawthorpe, R.L., Cowie, P.A., 2020. Transient landscape and stratigraphic responses to drainage integration in the actively extending central Italian Apennines. Geomorphology 353, 107013. https://doi.org/10.1016/j.geomorph.2019.107013

Goldsworthy, M., Jackson, J., 2000. Active normal fault evolution in Greece revealed by geomorphology and drainage

735   patterns. Journal of the Geological Society 157, 967–981. https://doi.org/10.1144/jgs.157.5.967

Griffin, B., Andi, Z., O'Reilly, S., Ryan, C., 1998. Phanerozoic evolution of the lithosphere beneath the Sino-Korean craton: Conference on Mantle Dynamics and Plate Interactions in East Asia. Mantle dynamics and plate interactions in east Asia, GEODYNAMICS SERIES 107–126.

Groves, K., Saville, C., Hurst, M.D., Jones, S.J., Song, S., Allen, M.B., 2020. Geomorphic expressions of collisional

740   tectonics in the Qilian Shan, north eastern Tibetan Plateau. Tectonophysics 788, 228503. https://doi.org/10.1016/j.tecto.2020.228503

Hack, J.T., 1957. Studies of longitudinal stream profiles in Virginia and Maryland. US Government Printing Office.

Hamdouni, R., Irigaray, C., Castillo, T., Chacón, J., Keller, E., 2008. Assessment of relative active tectonics, southwest border of the Sierra Nevada (southern Spain). Geomorphology 150–173. https://doi.org/10.1016/j.geomorph.2007.08.004

745   Harden, D.R., 1990. Controlling factors in the distribution and development of incised meanders in the central Colorado Plateau. GSA Bulletin 102, 233–242. https://doi.org/10.1130/0016-7606(1990)

He, J., Liu, M., Li, Y., 2003. Is the Shanxi rift of northern China extending? Geophysical research letters 30.

Heilman, E., Kolawole, F., Atekwana, E.A., Mayle, M., 2019. Controls of Basement Fabric on the Linkage of Rift Segments. Tectonics 38, 1337–1366. https://doi.org/10.1029/2018TC005362

750   Henstra, G.A., Rotevatn, A., Gawthorpe, R.L., Ravnås, R., 2015. Evolution of a major segmented normal fault during multiphase rifting: The origin of plan-view zigzag geometry. Journal of Structural Geology 74, 45–63. https://doi.org/10.1016/j.jsg.2015.02.005

Henza, A.A., Withjack, M.O., Schlische, R.W., 2011. How do the properties of a pre-existing normal-fault population influence fault development during a subsequent phase of extension? Journal of Structural Geology 33, 1312–1324.

755   https://doi.org/10.1016/j.jsg.2011.06.010

Hodge, M., Fagereng, Å., Biggs, J., 2018a. The Role of Coseismic Coulomb Stress Changes in Shaping the Hard Link Between Normal Fault Segments. Journal of Geophysical Research: Solid Earth 123, 797–814. https://doi.org/10.1002/2017JB014927

Hodge, M., Fagereng, Å., Biggs, J., Mdala, H., 2018b. Controls on early-rift geometry: New perspectives from the Bilila-Mtakataka Fault, Malawi. Geophysical Research Letters 45, 3896–3905.

Holdsworth, R.E., Stewart, M., Imber, J., Strachan, R.A., 2001. The structure and rheological evolution of reactivated continental fault zones: a review and case study. Geological Society, London, Special Publications 184, 115–137. https://doi.org/10.1144/GSL.SP.2001.184.01.07

Howell, L., Egan, S., Leslie, G., Clarke, S., Mitten, A., Pringle, J., 2020. The influence of low-density granite bodies on extensional basins. Geology Today 36, 22–26. https://doi.org/10.1111/gto.12297

Hu, X., Li, Y., Yang, J., 2005. Quaternary paleolake development in the Fen River basin, North China. Geomorphology 65, 1–13. https://doi.org/10.1016/j.geomorph.2004.06.008

Hu, X., Wang, L., Zhe, J., Lu, H., 2010. Morpho-Sedimentary evidence of the Huoshan Fault's late Cenozoic right-lateral movement in the Linfen Graben, Shanxi Graben System, North China. Front. Earth Sci. China 4, 311–319. https://doi.org/10.1007/s11707-010-0110-9

Jackson, J., Leeder, M., 1994. Drainage systems and the development of normal faults: an example from Pleasant Valley, Nevada. Journal of Structural Geology 16, 1041–1059. https://doi.org/10.1016/0191-8141(94)90051-5

Kattenhorn, S.A., Aydin, A., Pollard, D.D., 2000. Joints at high angles to normal fault strike: an explanation using 3-D numerical models of fault-perturbed stress fields. Journal of Structural Geology 22, 1–23. https://doi.org/10.1016/S0191-8141(99)00130-3

Kirby, E., Whipple, K.X., 2012. Expression of active tectonics in erosional landscapes. Journal of Structural Geology 44, 54–75. https://doi.org/10.1016/j.jsg.2012.07.009

Kolawole, F., Atekwana, E.A., Laó-Dávila, D.A., Abdelsalam, M.G., Chindandali, P.R., Salima, J., Kalindekafe, L., 2018. Active deformation of Malawi rift's north basin Hinge zone modulated by reactivation of preexisting Precambrian Shear zone fabric. Tectonics 37, 683–704.

Kolawole, F., Firkins, M.C., Al Wahaibi, T.S., Atekwana, E.A., Soreghan, M.J., 2021. Rift interaction zones and the stages of rift linkage in active segmented continental rift systems. Basin Research 33, 2984–3020.

Krabbendam, M., Barr, T.D., 2000. Proterozoic orogens and the break-up of Gondwana: why did some orogens not rift? Journal of African Earth Sciences 31, 35–49. https://doi.org/10.1016/S0899-5362(00)00071-3

Kusky, T., Li, J., Santosh, M., 2007. The Paleoproterozoic North Hebei Orogen: North China craton's collisional suture with the Columbia supercontinent. Gondwana Research, Tectonic evolution of China and adjacent crustal fragments 12, 4–28. https://doi.org/10.1016/j.gr.2006.11.012

Lambiase, J.J., Bosworth, W., 1995. Structural controls on sedimentation in continental rifts. Geological Society, London, Special Publications 80, 117–144. https://doi.org/10.1144/GSL.SP.1995.080.01.06

790 Leeder, M.R., Jackson, J.A., 1993. The interaction between normal faulting and drainage in active extensional basins, with examples from the western United States and central Greece. Basin Research 5, 79–102. https://doi.org/10.1111/j.1365-2117.1993.tb00059.x

Li, Y., Yang, J., Xia, Z., Mo, D., 1998. Tectonic geomorphology in the Shanxi Graben System, northern China. Geomorphology 23, 77–89. https://doi.org/10.1016/S0169-555X(97)00092-5

795 Liu, M., Cui, X., Liu, F., 2004. Cenozoic rifting and volcanism in eastern China: a mantle dynamic link to the Indo–Asian collision? Tectonophysics 393, 29–42.

Luo, Q., Li, Y., Schoenbohm, L., Rimando, J., Hu, X., Guo, A., Zhao, J., Li, X., Liu, Q., Jiang, S., Li, C., Sun, K., 2022. Direct Evidence for Dextral Shearing in the Shanxi Graben System: Geologic and Geomorphologic Constraints From the North Liulengshan Fault. Tectonics 41, e2022TC007490. https://doi.org/10.1029/2022TC007490

800 Maerten, L., 2000. Variation in slip on intersecting normal faults: Implications for paleostress inversion. Journal of Geophysical Research: Solid Earth 105, 25553–25565. https://doi.org/10.1029/2000JB900264

Makrari, S., Sharma, G., Taloor, A.K., Singh, M.S., Sarma, K.K., Aggarwal, S.P., 2022. Assessment of the geomorphic indices in relation to tectonics along selected sectors of Borpani River Basin, Assam using Cartosat DEM data. Geosystems and Geoenvironment 1, 100068. https://doi.org/10.1016/j.geogeo.2022.100068

805 McCaffrey, K.J.W., 1997. Controls on reactivation of a major fault zone: the Fair Head–Clew Bay line in Ireland. Journal of the Geological Society 154, 129–133. https://doi.org/10.1144/gsjgs.154.1.0129

McFadden, W.B.B., Leslie D., 1980. Tectonic Geomorphology North and South of the Garlock Fault, California, in: Geomorphology in Arid Regions. Routledge.

Menzies, M., Xu, Y., Zhang, H., Fan, W., 2007. Integration of geology, geophysics and geochemistry: A key to 810 understanding the North China Craton. Lithos, The Origin, Evolution and Present State of Continental Lithosphere 96, 1–21. https://doi.org/10.1016/j.lithos.2006.09.008

Menzies, M.A., Xu, Y., 1998. Geodynamics of the North China Craton, in: Mantle Dynamics and Plate Interactions in East Asia. American Geophysical Union (AGU), pp. 155–165. https://doi.org/10.1029/GD027p0155

Middleton, T.A., Elliott, J.R., Rhodes, E.J., Sherlock, S., Walker, R.T., Wang, W., Yu, J., Zhou, Y., 2017. Extension rates 815 across the northern Shanxi Grabens, China, from Quaternary geology, seismicity and geodesy. Geophysical Journal International 209, 535–558.

Middleton, T.A., Parsons, B., Walker, R.T., 2018. Comparison of seismic and geodetic strain rates at the margins of the Ordos Plateau, northern China. Geophysical Journal International 212, 988–1009.

Molnar, N., Cruden, A., Betts, P., 2020. The role of inherited crustal and lithospheric architecture during the evolution of the 820 Red Sea: Insights from three dimensional analogue experiments. Earth and Planetary Science Letters 544, 116377. https://doi.org/10.1016/j.epsl.2020.116377

Molnar, P., Tapponnier, P., 1975. Cenozoic Tectonics of Asia: Effects of a Continental Collision. Science 189, 419–426. https://doi.org/10.1126/science.189.4201.419

Moore, J.M., Davidson, A., 1978. Rift structure in southern Ethiopia. Tectonophysics 46, 159–173.
825   https://doi.org/10.1016/0040-1951(78)90111-7

Morley, C.K., 2010. Stress re-orientation along zones of weak fabrics in rifts: An explanation for pure extension in 'oblique' rift segments? Earth and Planetary Science Letters 297, 667–673. https://doi.org/10.1016/j.epsl.2010.07.022

Morley, C.K., 1988. Variable extension in Lake Tanganyika. Tectonics 7, 785–801. https://doi.org/10.1029/TC007i004p00785

830   Morley, C.K., Haranya, C., Phoosongsee, W., Pongwapee, S., Kornsawan, A., Wonganan, N., 2004. Activation of rift oblique and rift parallel pre-existing fabrics during extension and their effect on deformation style: examples from the rifts of Thailand. Journal of Structural Geology 26, 1803–1829. https://doi.org/10.1016/j.jsg.2004.02.014

Muirhead, J.D., Kattenhorn, S.A., 2018. Activation of preexisting transverse structures in an evolving magmatic rift in East Africa. Journal of Structural Geology 106, 1–18. https://doi.org/10.1016/j.jsg.2017.11.004

835   Mulaya, E., Gluyas, J., McCaffrey, K., Phillips, T., Ballentine, C., 2022. Structural geometry and evolution of the Rukwa Rift Basin, Tanzania: Implications for helium potential. Basin Research 34, 938–960. https://doi.org/10.1111/bre.12646

Obaid, A.K., Allen, M.B., 2019. Landscape expressions of tectonics in the Zagros fold-and-thrust belt. Tectonophysics 766, 20–30. https://doi.org/10.1016/j.tecto.2019.05.024

Peace, A., McCaffrey, K., Imber, J., Hunen, J. van, Hobbs, R., Wilson, R., 2018. The role of pre-existing structures during
840   rifting, continental breakup and transform system development, offshore West Greenland. Basin Research 30, 373–394. https://doi.org/10.1111/bre.12257

Pérez-Peña, J.V., Azañón, J.M., Booth-Rea, G., Azor, A., Delgado, J., 2009. Differentiating geology and tectonics using a spatial autocorrelation technique for the hypsometric integral. Journal of Geophysical Research: Earth Surface 114. https://doi.org/10.1029/2008JF001092

845   Perron, J.T., Royden, L., 2013. An integral approach to bedrock river profile analysis. Earth Surface Processes and Landforms 38, 570–576. https://doi.org/10.1002/esp.3302

Philippon, M., Willingshofer, E., Sokoutis, D., Corti, G., Sani, F., Bonini, M., Cloetingh, S., 2015. Slip re-orientation in oblique rifts. Geology 43, 147–150.

Phillips, T.B., Jackson, C.A., Bell, R.E., Duffy, O.B., Fossen, H., 2016. Reactivation of intrabasement structures during
850   rifting: A case study from offshore southern Norway. Journal of Structural Geology 91, 54–73.

Phillips, T.B., McCaffrey, K.J.W., 2019. Terrane Boundary Reactivation, Barriers to Lateral Fault Propagation and Reactivated Fabrics: Rifting Across the Median Batholith Zone, Great South Basin, New Zealand. Tectonics 38, 4027–4053. https://doi.org/10.1029/2019TC005772

Phillips, T.B., Naliboff, J.B., McCaffrey, K.J.W., Pan, S., van Hunen, J., Froemchen, M., 2023. The influence of crustal
855   strength on rift geometry and development – insights from 3D numerical modelling. Solid Earth 14, 369–388. https://doi.org/10.5194/se-14-369-2023

Qi, J., Yang, Q., 2010. Cenozoic structural deformation and dynamic processes of the Bohai Bay basin province, China. Marine and Petroleum Geology 27, 757–771. https://doi.org/10.1016/j.marpetgeo.2009.08.012

Reeve, M.T., Bell, R.E., Duffy, O.B., Jackson, C.A.-L., Sansom, E., 2015. The growth of non-colinear normal fault systems; What can we learn from 3D seismic reflection data? Journal of Structural Geology 70, 141–155.

Ring, U., 1994. The influence of preexisting structure on the evolution of the Cenozoic Malawi rift (East African rift system). Tectonics 13, 313–326. https://doi.org/10.1029/93TC03188

Rosendahl, B.R., 1987. Architecture of Continental Rifts with Special Reference to East Africa. Annual Review of Earth and Planetary Sciences 15, 445–503. https://doi.org/10.1146/annurev.ea.15.050187.002305

Rotevatn, A., Jackson, C.A.-L., Tvedt, A.B., Bell, R.E., Blækkan, I., 2019. How do normal faults grow? Journal of Structural Geology 125, 174–184.

Samsu, A., Cruden, A.R., Hall, M., Micklethwaite, S., Denyszyn, S.W., 2019. The influence of basement faults on local extension directions: Insights from potential field geophysics and field observations. Basin Research 31, 782–807. https://doi.org/10.1111/bre.12344

Samsu, A., Cruden, A.R., Micklethwaite, S., Grose, L., Vollgger, S.A., 2020. Scale matters: The influence of structural inheritance on fracture patterns. Journal of Structural Geology 130, 103896. https://doi.org/10.1016/j.jsg.2019.103896

Samsu, A., Cruden, A.R., Molnar, N.E., Weinberg, R.F., 2021. Inheritance of penetrative basement anisotropies by extension-oblique faults: Insights from analogue experiments. Tectonics 40, e2020TC006596.

Samsu, A., Micklethwaite, S., Williams, J., Fagereng, A., Cruden, A.R., 2022. A review of structural inheritance in rift basin formation.

Schellart, W.P., Chen, Z., Strak, V., Duarte, J.C., Rosas, F.M., 2019. Pacific subduction control on Asian continental deformation including Tibetan extension and eastward extrusion tectonics. Nat Comm. 10, 4480. https://doi.org/10.1038/s41467-019-12337-9

Schiffer, C., Doré, A.G., Foulger, G.R., Franke, D., Geoffroy, L., Gernigon, L., Holdsworth, B., Kusznir, N., Lundin, E., McCaffrey, K., Peace, A.L., Petersen, K.D., Phillips, T.B., Stephenson, R., Stoker, M.S., Welford, J.K., 2020. Structural inheritance in the North Atlantic. Earth-Science Reviews, A new paradigm for the North Atlantic Realm 206, 102975. https://doi.org/10.1016/j.earscirev.2019.102975

Schmidt, K.M., Montgomery, D.R., 1995. Limits to Relief. Science 270, 617–620. https://doi.org/10.1126/science.270.5236.617

Scholz, C.H., 1982. Scaling laws for large earthquakes: Consequences for physical models. Bulletin of the Seismological Society of America 72, 1–14. https://doi.org/10.1785/BSSA0720010001

Scholz, C.A., 1995. Deltas of the Lake Malawi Rift, East Africa: Seismic Expression and Exploration Implications 1. AAPG Bulletin 79, 1679–1697. https://doi.org/10.1306/7834DE54-1721-11D7-8645000102C1865D

Schumacher, M.E., 2002. Upper Rhine Graben: Role of preexisting structures during rift evolution. Tectonics 21, 6-1-6–17. https://doi.org/10.1029/2001TC900022

Schwanghart, W., Scherler, D., 2014. Short Communication: TopoToolbox 2 – MATLAB-based software for topographic analysis and modeling in Earth surface sciences. Earth Surface Dynamics 2, 1–7. https://doi.org/10.5194/esurf-2-1-2014

Şengör, A.M.C., Lom, N., Sağdıç, N.G., 2019. Tectonic inheritance, structure reactivation and lithospheric strength: the relevance of geological history. Geological Society, London, Special Publications 470, 105–136.

895   https://doi.org/10.1144/SP470.8

Shanxi Bureau of Geology and Mineral Resources (SBGMR), 1989, Regional Geology of Shanxi Province: Beijing, China, Geological Publishing House, 780 p.

Shen, Z.-K., Zhao, C., Yin, A., Li, Y., Jackson, D.D., Fang, P., Dong, D., 2000. Contemporary crustal deformation in east Asia constrained by Global Positioning System measurements. Journal of Geophysical Research: Solid Earth 105, 5721–

900   5734. https://doi.org/10.1029/1999JB900391

Shi, W., Cen, M., Chen, L., Wang, Y., Chen, X., Li, J., Chen, P., 2015a. Evolution of the late Cenozoic tectonic stress regime in the Shanxi Rift, central North China Plate inferred from new fault kinematic analysis. Journal of Asian Earth Sciences, Active Tectonics and Meso-Cenozoic Intraplate Deformation in North China Block 114, 54–72. https://doi.org/10.1016/j.jseaes.2015.04.044

905   Shi, W., Dong, S., Hu, J., 2020. Neotectonics around the Ordos Block, North China: A review and new insights. Earth-Science Reviews 200, 102969.

Shi, W., Dong, S., Liu, Y., Hu, J., Chen, X., Chen, P., 2015b. Cenozoic tectonic evolution of the South Ningxia region, northeastern Tibetan Plateau inferred from new structural investigations and fault kinematic analyses. Tectonophysics 649, 139–164. https://doi.org/10.1016/j.tecto.2015.02.024

910   Snyder, N.P., Whipple, K.X., Tucker, G.E., Merritts, D.J., 2000. Landscape response to tectonic forcing: Digital elevation model analysis of stream profiles in the Mendocino triple junction region, northern California. Geological Society of America Bulletin 112, 1250–1263.

Storchak, D.A., D. Di Giacomo, I. Bondár, E.R. Engdahl, J. Harris, W.H.K. Lee, A. Villaseñor and P. Bormann (2013). Public Release of the ISC-GEM Global Instrumental Earthquake Catalogue (1900-2009). Seism. Res. Lett., 84, 5, 810-815,

915   doi: 10.1785/0220130034.

Storchak, D.A., D. Di Giacomo, E.R. Engdahl, J. Harris, I. Bondár, W.H.K. Lee, P. Bormann and A. Villaseñor (2015). The ISC-GEM Global Instrumental Earthquake Catalogue (1900-2009): Introduction, Phys. Earth Planet. Int., 239, 48-63, doi: 10.1016/j.pepi.2014.06.009.

Strahler, A.N., 1957. Quantitative analysis of watershed geomorphology. Eos, Transactions American Geophysical Union

920   38, 913–920. https://doi.org/10.1029/TR038i006p00913

Strahler, A.N., 1952. Hypsometirc (area-altitude) Analysis of erosional topography. GSA Bulletin 63, 1117–1142. https://doi.org/10.1130/0016-7606(1952)63[1117:HAAOET]2.0.CO;2

Su, P., He, H., Tan, X., Liu, Y., Shi, F., Kirby, E., 2021. Initiation and evolution of the Shanxi Rift System in North China: Evidence from low-temperature thermochronology in a plate reconstruction framework. Tectonics 40, e2020TC006298.

925 Tang Y.-C., Fen Y.-G., Chen Zhongshun J., Zhou S.-Y., Ning J.-Y., Wei S.-Q., Li P., Chun-Quan Y., Fan W.-Y., Wang H.-Y., 2010. Receiver function analysis at Shanxi Rift. Chinese Journal of Geophysics 53, 2102–2109. https://doi.org/10.3969/j.issn.0001-5733.2010.09.010

Su, P., He, H., Liu, Y., Shi, F., Granger, D.E., Kirby, E., Luo, L., Han, F., Lu, R., 2023. Quantifying the Structure and Extension Rate of the Linfen Basin, Shanxi Rift System Since the Latest Miocene: Implications for Continental Magma-Poor 930 Rifting. Tectonics 42, e2023TC007885. https://doi.org/10.1029/2023TC007885

Tapponnier, P., Molnar, P., 1977. Active faulting and tectonics in China. Journal of Geophysical Research (1896-1977) 82, 2905–2930. https://doi.org/10.1029/JB082i020p02905

Taylor, S.K., Bull, J.M., Lamarche, G., Barnes, P.M., 2004. Normal fault growth and linkage in the Whakatane Graben, New Zealand, during the last 1.3 Myr. Journal of Geophysical Research: Solid Earth 109. https://doi.org/10.1029/2003JB002412

935 Tommasi, A., Vauchez, A., 2001. Continental rifting parallel to ancient collisional belts: an effect of the mechanical anisotropy of the lithospheric mantle. Earth and Planetary Science Letters 185, 199–210. https://doi.org/10.1016/S0012-821X(00)00350-2

Trap, P., Faure, M., Lin, W., Bruguier, O., Monié, P., 2008. Contrasted tectonic styles for the Paleoproterozoic evolution of the North China Craton. Evidence for a ~2.1Ga thermal and tectonic event in the Fuping Massif. Journal of Structural 940 Geology 30, 1109–1125. https://doi.org/10.1016/j.jsg.2008.05.001

Trap, P., Faure, M., Lin, W., Meffre, S., 2009a. The Lüliang Massif: a key area for the understanding of the Palaeoproterozoic Trans-North China Belt, North China Craton. Geological Society, London, Special Publications 323, 99–125.

Trap, P., Faure, M., Lin, W., Monié, P., 2007. Late Paleoproterozoic (1900–1800Ma) nappe stacking and polyphase 945 deformation in the Hengshan–Wutaishan area: Implications for the understanding of the Trans-North-China Belt, North China Craton. Precambrian Research 156, 85–106. https://doi.org/10.1016/j.precamres.2007.03.001

Trap, P., Faure, M., Lin, W., Monié, P., Meffre, S., Melleton, J., 2009b. The Zanhuang Massif, the second and eastern suture zone of the Paleoproterozoic Trans-North China Orogen. Precambrian Research 172, 80–98.

Vauchez, A., Barruol, G., Tommasi, A., 1997. Why do continents break-up parallel to ancient orogenic belts? Terra Nova 9, 950 62–66. https://doi.org/10.1111/j.1365-3121.1997.tb00003.x

Versfelt, J., Rosendahl, B.R., 1989. Relationships between pre-rift structure and rift architecture in Lakes Tanganyika and Malawi, East Africa. Nature 337, 354–357. https://doi.org/10.1038/337354a0

Vetel, W., Le Gall, B., 2006. Dynamics of prolonged continental extension in magmatic rifts: the Turkana Rift case study (North Kenya). Geological Society, London, Special Publications 259, 209–233. 955 https://doi.org/10.1144/GSL.SP.2006.259.01.17

Wedmore, L.N.J., Williams, J.N., Biggs, J., Fagereng, Å., Mphepo, F., Dulanya, Z., Willoughby, J., Mdala, H., Adams, B.A., 2020. Structural inheritance and border fault reactivation during active early-stage rifting along the Thyolo fault, Malawi. Journal of Structural Geology 139, 104097. https://doi.org/10.1016/j.jsg.2020.104097

Whipple, K.X., 2004. Bedrock rivers and the geomorphology of active orogens. Annu. Rev. Earth Planet. Sci. 32, 151–185.

960   https://doi.org/10.1146/annurev.earth.32.101802.120356

Whittaker, A.C., 2012. How do landscapes record tectonics and climate? Lithosphere 4, 160–164.

Whittaker, A.C., Attal, M., Cowie, P.A., Tucker, G.E., Roberts, G., 2008. Decoding temporal and spatial patterns of fault uplift using transient river long profiles. Geomorphology 100, 506–526. https://doi.org/10.1016/j.geomorph.2008.01.018

Williams, J.N., Fagereng, Å., Wedmore, L.N., Biggs, J., Mphepo, F., Dulanya, Z., Mdala, H., Blenkinsop, T., 2019. How do

965   variably striking faults reactivate during rifting? Insights from southern Malawi. Geochemistry, Geophysics, Geosystems 20, 3588–3607.

Wilson, J.T., 1966. Did the Atlantic Close and then Re-Open? Nature 211, 676–681. https://doi.org/10.1038/211676a0

Wilson, R.W., Holdsworth, R.E., Wild, L.E., McCaffrey, K.J.W., England, R.W., Imber, J., Strachan, R.A., 2010. Basement-influenced rifting and basin development: a reappraisal of post-Caledonian faulting patterns from the North Coast Transfer

970   Zone, Scotland. Geological Society, London, Special Publications 335, 795–826. https://doi.org/10.1144/SP335.32

Wobus, C., Whipple, K.X., Kirby, E., Snyder, N., Johnson, J., Spyropolou, K., Crosby, B., Sheehan, D., 2006. Tectonics from topography: Procedures, promise, and pitfalls, in: Willett, S.D., Hovius, N., Brandon, M.T., Fisher, D.M. (Eds.), Tectonics, Climate, and Landscape Evolution. Geological Society of America, p. 0. https://doi.org/10.1130/2006.2398(04)

Wong, W.H., 1927. Crustal Movements and Igneous Activities in Eastern China Since Mesozoic Time.1. Bulletin of the

975   Geological Society of China 6, 9–37. https://doi.org/10.1111/j.1755-6724.1927.mp6001002.x

Xu, X., 1990. The Features of Later Quaternary Activity of the Piedmont Fault of Mt. Huoshan, Shanxi Province and 1303 Hongdong Earthquake (M=8). Seismology and Geology 12, 21–30.

Xu, X., Ma, X., 1992. Geodynamics of the Shanxi rift system, China. Tectonophysics 208, 325–340.

Xu, X., Ma, X., Deng, Q., 1993. Neotectonic activity along the Shanxi rift system, China. Tectonophysics 219, 305–325.

980   Xu, Y., He, H., Deng, Q., Allen, M.B., Sun, H., Bi, L., 2018. The CE 1303 Hongdong Earthquake and the Huoshan Piedmont Fault, Shanxi Graben: Implications for Magnitude Limits of Normal Fault Earthquakes. J. Geophys. Res. Solid Earth 123, 3098–3121. https://doi.org/10.1002/2017JB014928

Zhai, M., Li, T.-S., Peng, P., Hu, B., Liu, F., Zhang, Y., n.d. Precambrian key tectonic events and evolution of the North China craton. https://doi.org/10.1144/SP338.12

985   Zhai, M.-G., Santosh, M., 2011. The early Precambrian odyssey of the North China Craton: A synoptic overview. Gondwana Research, Precambrian geology and tectonic evolution of the North China Craton 20, 6–25. https://doi.org/10.1016/j.gr.2011.02.005

Zhang, C., Li, C., Deng, H., Liu, Y., Liu, L., Wei, B., Li, H., Liu, Z., 2011. Mesozoic contraction deformation in the Yanshan and northern Taihang mountains and its implications to the destruction of the North China Craton. Sci. China Earth

990   Sci. 54, 798–822. https://doi.org/10.1007/s11430-011-4180-7

Zhang, Y., Dong, S., Zhao, Y., Zhang, T., 2008. Jurassic Tectonics of North China: A Synthetic View. Acta Geologica Sinica - English Edition 82, 310–326. https://doi.org/10.1111/j.1755-6724.2008.tb00581.x

Zhang, Y., Ma, Y., Yang, N., Shi, W., Dong, S., 2003. Cenozoic extensional stress evolution in North China. Journal of Geodynamics 36, 591–613. https://doi.org/10.1016/j.jog.2003.08.001

995 Zhang, Y.Q., Mercier, J.L., Vergély, P., 1998. Extension in the graben systems around the Ordos (China), and its contribution to the extrusion tectonics of south China with respect to Gobi-Mongolia. Tectonophysics 285, 41–75. https://doi.org/10.1016/S0040-1951(97)00170-4

Zhao, G., Min, S., Wilde, S.A., Sanzhong, L., 2005. Late Archean to Paleoproterozoic evolution of the North China Craton: key issues revisited. Precambrian Research 136, 177–202. https://doi.org/10.1016/j.precamres.2004.10.002

1000 Zhao, L., Zheng, T., 2005. Using shear wave splitting measurements to investigate the upper mantle anisotropy beneath the North China Craton: Distinct variation from east to west. Geophysical Research Letters 32. https://doi.org/10.1029/2005GL022585

Zhu, R., Xu, Y., Zhu, G., Zhang, H., Xia, Q., Zheng, T., 2012. Destruction of the North China Craton. Sci. China Earth Sci. 55, 1565–1587. https://doi.org/10.1007/s11430-012-4516-y

1005 Ziegler, P.A., Cloetingh, S., 2004. Dynamic processes controlling evolution of rifted basins. Earth-Science Reviews 64, 1–50. https://doi.org/10.1016/S0012-8252(03)00041-2

Zwaan, F., Chenin, P., Erratt, D., Manatschal, G., Schreurs, G., 2022. Competition between 3D structural inheritance and kinematics during rifting: Insights from analogue models. Basin Research 34, 824–854. https://doi.org/10.1111/bre.12642

Zwaan, F., Schreurs, G., 2017. How oblique extension and structural inheritance influence rift segment interaction: Insights 1010 from 4D analog models. Interpretation 5, SD119–SD138. https://doi.org/10.1190/INT-2016-0063.1

Zwaan, F., Schreurs, G., Naliboff, J., Buiter, S.J.H., 2016. Insights into the effects of oblique extension on continental rift interaction from 3D analogue and numerical models. Tectonophysics, Special issue on Tectonics of oblique plate boundary systems 693, 239–260. https://doi.org/10.1016/j.tecto.2016.02.036